PLD1 promotes spindle assembly and migration through regulating autophagy in mouse oocyte meiosis

Jiaqi Zhang, Ying Tian, Xiangning Xu, Bicheng Wang, Ziqi Huang, Ke Song, Shuo Lou, Jingyi Kang, Ningning Zhang, Jingyu Li, Jing Weng, Yuanjing Liang & Wei Ma

View supplementary material

Published online: 27 Mar 2024.

Submit your article to this journal

Article views: 37

View related articles

View Crossmark data

Taylor & Francis
Taylor & Francis Group

RESEARCH PAPER

Check for updates

PLD1 promotes spindle assembly and migration through regulating autophagy in mouse oocyte meiosis

Jiaqi Zhang[a], Ying Tian[a], Xiangning Xu[a], Bicheng Wang[a], Ziqi Huang[a], Ke Song[b], Shuo Lou[a], Jingyi Kang[a], Ningning Zhang[a], Jingyu Li[b], Jing Weng[a], Yuanjing Liang[a], and Wei Ma[a]

[a]Department of Histology and Embryology, School of Basic Medical Sciences, Capital Medical University, Beijing, China; [b]Department of Human Reproductive Medicine, Beijing Obstetrics and Gynecology Hospital, Capital Medical University, Beijing, China

ABSTRACT

PLD1 has been implicated in cytoskeletal reorganization and vesicle trafficking in somatic cells; however, its function remains unclear in oocyte meiosis. Herein, we found PLD1 stably expresses in mouse oocytes meiosis, with direct interaction with spindle, RAB11A$^+$ vesicles and macroautophagic/autophagic vacuoles. The genetic or chemical inhibition of PLD1 disturbed MTOC clustering, spindle assembly and its cortical migration, also decreased PtdIns(4,5)P$_2$, phosphorylated CFL1 (p-CFL1 [Ser3]) and ACTR2, and their local distribution on MTOC, spindle and vesicles. Furthermore in PLD1-suppressed oocytes, vesicle size was significantly reduced while F-actin density was dramatically increased in the cytoplasm, the asymmetric distribution of autophagic vacuoles was broken and the whole autophagic process was substantially enhanced, as illustrated with characteristic changes in autophagosomes, autolysosome formation and levels of ATG5, BECN1, LC3-II, SQSTM1 and UB. Exogenous administration of PtdIns(4,5)P$_2$ or overexpression of CFL1 hyperphosphorylation mutant (CFL1^{S3E}) could significantly improve polar MTOC focusing and spindle structure in PLD1-depleted oocytes, whereas overexpression of ACTR2 could rescue not only MTOC clustering, and spindle assembly but also its asymmetric positioning. Interestingly, autophagy activation induced similar defects in spindle structure and positioning; instead, its inhibition alleviated the alterations in PLD1-depleted oocytes, and this was highly attributed to the restored levels of PtdIns(4,5)P$_2$, ACTR2 and p-CFL1 (Ser3). Together, PLD1 promotes spindle assembly and migration in oocyte meiosis, by maintaining rational levels of ACTR2, PtdIns(4,5)P$_2$ and p-CFL1 (Ser3) in a manner of modulating autophagy flux. This study for the first time introduces a unique perspective on autophagic activity and function in oocyte meiotic development.

Abbreviations: ACTR2/ARP2: actin related protein 2; ACTR3/ARP3: actin related protein 3; ATG5: autophagy related 5; Baf-A1: bafilomycin A$_1$; BFA: brefeldin A; GAPDH: glyceraldehyde-3-phosphate dehydrogenase; GOLGA2/GM130: golgin A2; GV: germinal vesicle; GVBD: germinal vesicle breakdown; IVM: *in vitro* maturation; MAP1LC3/LC3: microtubule-associated protein 1 light chain 3; MI: metaphase of meiosis I; MII: metaphase of meiosis II; MO: morpholino; MTOC: microtubule-organizing center; MTOR: mechanistic target of rapamycin kinase; PB1: first polar body; PLA: proximity ligation assay; PLD1: phospholipase D1; PtdIns(4,5)P$_2$/PIP2: phosphatidylinositol 4,5-bisphosphate; RAB11A: RAB11A, member RAS oncogene family; RPS6KB1/S6K1: ribosomal protein S6 kinase B1; SQSTM1/p62: sequestosome 1; TEM: transmission electron microscopy; TUBA/α-tubulin: tubulin alpha; TUBG/γ-tubulin: tubulin gamma; UB: ubiquitin; WASL/N-WASP: WASP like actin nucleation promoting factor

Introduction

The meiotic maturation of mammalian oocytes involves two consecutive asymmetric divisions. In each division, half of the chromosomes are extruded into a tiny polar body (PB), so as to retain the majority of cytoplasmic storage materials for the following embryo development after fertilization [1,2]. Such extraordinary inequality of cytokinesis is determined by spindle cortial migration and asymmetric positioning [3], a process not dependent on microtubules, but rather, on dynamic F-actin networks [4–6]. The motility of F-actin network is essentially modulated by RAB11A (RAB11A, member RAS oncogene family)-positive vesicles in the cytoplasm because the actin nucleators, including FMN2/formin 2 and

the ACTR2/ARP2 (actin related protein 2)-ACTR3/ARP3 (actin related protein 3) complex, are clustered and sequestered on these vesicles. Defective vesicle fusion, fission or outward-directed dynamics will affect the density, mobility and cortical connection of F-actin meshwork, preventing spindle migration [7–9]. The assembly of oocyte spindle is an acentrosomal process and governed by unique microtubule organizing centers (MTOCs) [10]. Abnormalities in MTOCs will impact spindle assembly and chromosome aligment, which may increase the risk of aneuploidy [11]. CFL1 (cofilin 1), an actin-severing protein, participates in the process of centrosome clustering (CC) in somatic cells, with the help of phosphatidylinositol 4,5-bisphosphate PtdIns (4,5)P$_2$ [12,13].

Until now, it is still not fully identified about the molecules and pathways which regulate vesicle dynamics and MTOC clustering in oocyte meiosis.

Macroautophagy/autophagy is a biological process that plays a housekeeping role in eukaryotic cells for the degradation and recycling of biological macromolecules or damaged organelles [14,15]. The chemical blocking of MTOR (mechanistic target of rapamycin kinase), a negative regulating factor for autophagic activation, could delay spindle migration in mouse oocytes [16], preliminarily suggesting autophagy activity may be negatively associated with spindle cortical migration. Furthermore, enhanced autophagy activity is found to disturb centrosome integrity in U2OS cells [17]. It is necessary to reveal whether autophagy activity involves in MTOCs clustering and maintenance during oocyte meiotic progression.

PLD1 (phospholipase D1) is a widely distributed kind of enzyme found in bacteria, fungi, plants and animals [18,19]. The structure of PLD1 consists of phox homology (PX) and pleckstrin homology (PH) domains in the N-terminal regulatory region and two characteristic conserved HKD catalytic domains in the C-terminal catalytic region, and also a conserved LOOP domain between two HKD domains. The HKD motifs are essential for PLD1 catalysis and dimerization, primarily hydrolyze the membrane-lipid phosphatidylcholine (PC) into signal molecule phosphatidic acid (PA) and soluble choline [18,20]. PLD1 has been implicated in several important cellular functions that require membrane remodeling or biogenesis, such as vesicular transportation, endocytosis, degranulation and cell cycle progression [21–23], but it is still unknown about PLD1 phase-specific role in mitotic or meiotic cells. PLD1 activity is regulated particularly by their interaction with inositol phospholipids, small GTPases of the ARF and RHO families, and PRKC (protein kinase C) isoforms [24]. The PH domain of PLD1, especially is PtdIns(4,5)P_2 specific, has emerged as important regulators of actin dynamics, directly regulates the activities and subcellular localizations of numerous actin-binding proteins. PLD1 also interacts directly with cytoskeleton proteins, such as actin, tubulin and CFL1 [22,25,26]. There are full proof that PLD1 is a critical regulator in the activation of MTOR signaling by a variety of stimuli, thus supporting PLD1 as a limiting factor for autophagy activity in somatic cells, but this assumption is not universal, PLD1 still has been postulated both as a positive as well as a negative autophagy modulator, depending on cell types or molecular events [27–32]. Up to now, the exact role of PLD1 in oocyte meiosis is a complete unstudied research field, and also it is totally not known about the exact physiological function of autophagic process during oocyte meiotic division.

In the present study, we found that PLD1 is stably expressed and distributed on spindle, cytoplasmic vesicles and autophagic vacuoles in mouse oocytes during meiotic progression, PLD1 works to maintain rational levels of ACTR2, PtdIns(4,5)P_2 and p-CFL1 (Ser3) by modulating autophagic flux in oocytes, thereby facilitates MTOCs clustering, spindle assembly and its asymmetric positioning.

Results

PLD1 expression and subcellular localization in mouse oocyte meiosis

To investigate the role of PLD1 during meiotic maturation in mouse oocytes, its protein expression and subcellular location pattern were initially detected. As illustrated by western blot procedure, PLD1 was stably detected at a high level in oocytes at different meiotic stages (Figure 1A). Immunofluorescence demonstrated that PLD1 was mainly aggregated as multi large foci in the surrounding area of nuclei at meiotic prophase (germinal vesicle stage, GV) (Figure 1B [a-d]), and distributed in two forms after GVBD, that is, some PLD1 was colocalized with the microtubules from GVBD to metaphase of meiosis II (MII), and precisely overlapped with the spindle apparatus at metaphase of meiosis I (MI) and MII stage (Figure 1B [e-t]), while the other portion of PLD1 signals were labeled on GOLGA2/GM130 (golgin A2)-positive vesicles, as showed in (Figure 1C). These data may suggest PLD1 potential involvement in meiotic spindle formation and vesicle-modulated positioning in mouse oocytes meiosis.

Blocking PLD1 destroyed MTOC clustering, spindle assembly and migration

We further investigated the exact role of PLD1 in vesicle dynamics, and spindle assembly and migration through blocking PLD1 with genetic or chemical approaches. The specific *Pld1* morpholino (MO) oligo was injected into GV oocytes to block the translation of endogenous *Pld1* mRNA. The western blot and quantitative statistical analysis illustrated that the protein level of PLD1 was significantly reduced in MO group (Figure 2A). This also confirmed the specificity of MO and the efficiency of our micromanipulation. In addition, the *Myc-Pld1* cRNA produced *in vitro* was effectively translated in oocytes and properly rescued PLD1 protein level in *Pld1*-MO-injected oocytes (Figure 2B). As showed in Figure S1A, PLD1 knockdown did not impact the timely occurrence of GVBD in mouse oocytes, making no distinguishable difference between groups of control, MO and MO + *Myc-Pld1* cRNA at 1 h, 1.5 h and 2 h of *in vitro* culture. In line with this, the statistical analysis demonstrated no significant delay in meiotic resumption of oocytes incubated with VU 0155069 (hereinafter referred to as VU), a specific inhibitor of PLD1, at concentrations of 1, 2.5, 5, 7.5, 10, 12.5 and 15 μM compared to the DMSO control (Figure S1B).

Evidently, abnormal spindle structure and positioning were observed in MI oocytes with PLD1 inhibition or depletion. As showed in (Figure 2D), to quantitatively compare changes in oocytes, we conducted immunofluorescence on oocytes at MI stage, and measured the value of long axis length of spindle (l), oocyte spherical radius (R), the distance between spindle center and oocyte spherical center (d1) and the width of chromosome region (d2) in
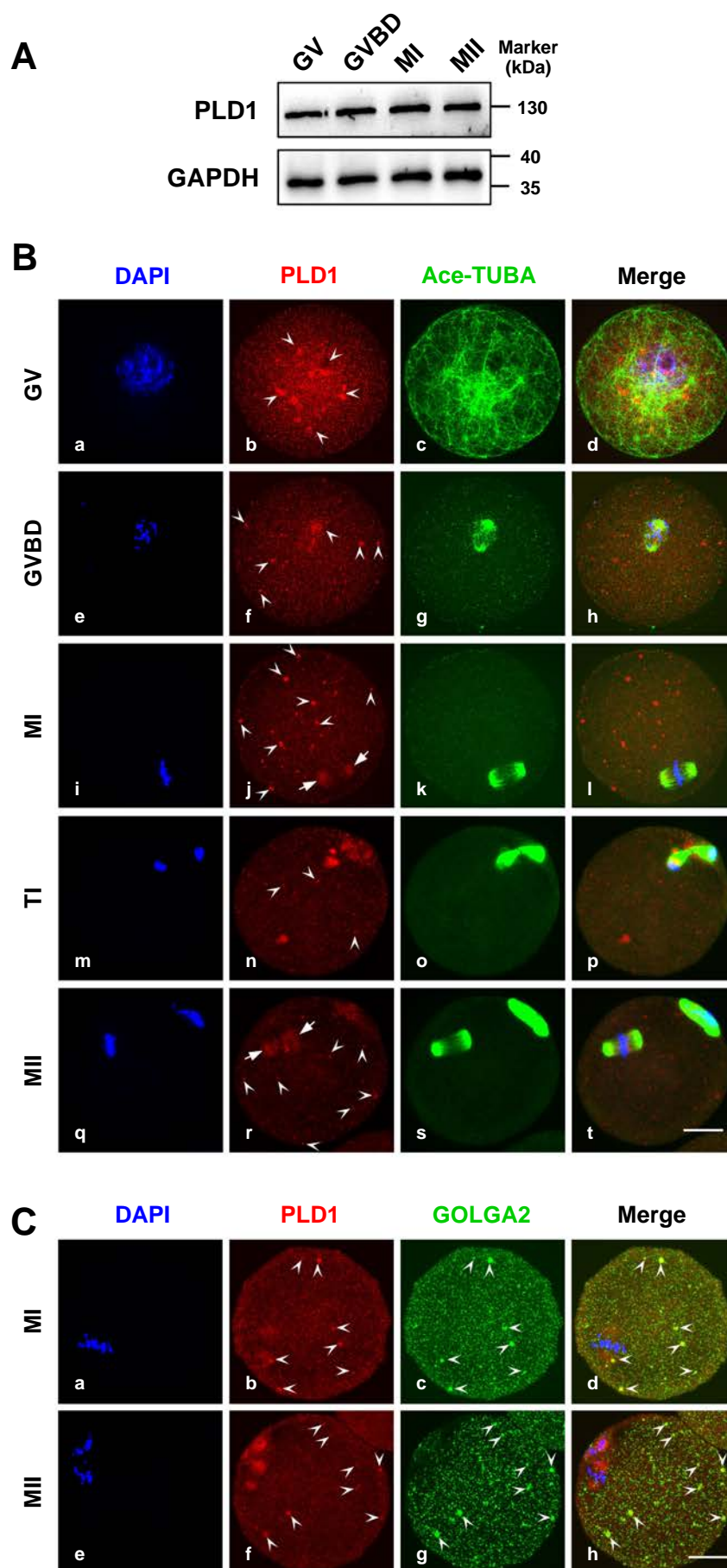
Figure 1. Expression and subcellular localization of PLD1 in mouse oocytes during meiosis. (A) Western blot analysis detected stable expression of PLD1. Each sample contained 90 cells which were collected after 0, 2, 8 and 16 h *in vitro* maturation (IVM) culture, corresponding to GV, GVBD, MI and MII. (B) Representative

each oocyte. Accordingly, the ratio of "l" to "R" (I/R) indicates the relative value of spindle length, "d1" to "R" (d1/R) represents the relative value of spindle migrating distance, and "d2" to "R" (d2/R) stands for the relative width value of chromosome region. As showed with the representative images in Figure 2C, enlarged and un-symmetrical spindles were frequently observed in PLD1-knocked down oocytes, which were not properly positioned in the cortical area, and obviously the chromosomes were not neatly aligned in linear manner on the metaphase plate. The quantification statistics confirmed the proportion of asymmetric spindle was significantly higher in *Pld1* MO group than in control (Figure 2E), and concurrently, the relative values of both spindle size and spindle length were dramatically increased (Figure 2F,G). Interestingly, the stability of microtubules, and the attachment between chromosome kinetochores and microtubules (KT-MT attachment) were not influenced by the loss of PLD1 (data not showed). The width of chromosome region, showed by the value of "d2/R", was also evidently augmented (Figure 2H), indicating chromosomes malalignment caused by PLD1 knockdown. In logic consistence with spindle abnormalities, MTOCs were not tightly clustered but distributed over a pretty large area in spindle poles, as labeled with TUBG/γ-tubulin (tubulin gamma) (Figure 2C), and statistical analysis showed the proportion of oocytes with defocused MTOCs was significantly higher (Figure 2I), and further the number of polar MTOC foci was also markedly elevated (Figure 2J) in *Pld1* MO group than control group. In addition, the value of "d1/R" was markedly reduced by *Pld1* MO (Figure 2K), clearly illustrating delayed spindle migrating to cortex area. More importantly, all the abnormal phenotypes could be dramatically reversed by microinjected exogenous *Pld1* cRNA (Figure 2C–K), supporting essential role of PLD1 in spindle assembly and migration in oocytes. This assumption is supported by further evidence from inhibitor treatment experiment, as showed in Figure S2, VU imposed negative influences on MTOC, spindle and chromosome alignment in a dose-dependent manner, causing phenotype consistent with *Pld1* MO treatment. Together, these data suggest PLD1 is required for oocyte spindle organization and cortical positioning.

Blocking PLD1 disturbed oocyte asymmetric division, producing large PB1

As the suppression of PLD1 influenced spindle migration in oocytes, we further investigated whether PLD1 loss impacts the asymmetric cytokinesis and the extrusion of first polar body (PB1) during the first meiotic division. After oocytes were cultured for 16 h, small PB1s were usually extruded and located in the perivitelline space of oocytes in control group, in contrast, large PB1 was frequently observed in VU group, even some MII oocytes looked like 2-cell embryos because of the huge size of PB1s (Figure 3A,B), suggesting the asymmetry

of cytokinesis was disturbed. Statistical analysis demonstrated that VU administration significantly increased the volume of PB1 in a dose-dependent manner (Figure 3C). In addition, we found the extrusion of PB1 was blocked by higher concentration of VU, with a decreased MII rate in 7.5 μM and 10 μM VU groups compared to DMSO group (Figure 3D).

Same as results of VU treatment, PLD1 knockdown by MO also gave rise to the production of large PB1s in oocytes cultured for 16 h, however, the volume of PB1 could be effectively rectified toward the normal level by *Pld1* cRNA microinjection (Figure 3E–G). Interestingly, the depletion of PLD1 didn't influence PB1 extrusion (Figure 3H), actually, this can be logically explained by the fact that PLD1 inhibition did not affect the KT-MT attachments and the activation of spindle assembly checkpoint in oocytes (data not showed) [11]. Collectively, these results suggests that PLD1 participates in the regulation of asymmetric division in mouse oocytes.

Suppressing PLD1 destroyed vesicle morphological dynamics in mouse oocytes

Based on above data, we propose that PLD1 may function in spindle asymmetric positioning through regulating the morphological dynamics of vesicles in oocyte meiosis. As expected, the number of large RAB11A-positive vesicles (>1000 pixels) were decreased, on the contrary the population of small RAB11A-positive vesicles (<1000 pixels) were increased in oocytes injected with *Pld1* MO. Noteworthy is that, this change pattern could be effectively reversed by exogenous *Pld1* cRNA (Figure 4A–C). It is generally accepted that complete Golgi apparatus stacks will convert into Golgi apparatus-like clusters of small membrane fragments and vesicles as oocytes enter metaphase [33,34], so transmission electron microscopy (TEM) was used to further observe morphological features of vesicles and Golgi apparatus-like clusters in oocytes with PLD1 depletion. Firstly, we counted up large vesicles (maximum diameter >0.2 μm) and small ones (maximum diameter 0.1 μm-0.2 μm) per 3 μm × 3 μm area in oocytes. Consistent with data of immunofluorescence, TEM analysis again revealed decreased number of large vesicles but simultaneously, increased proportion of small vesicles after PLD1 knockdown, and definitely this change trend was significantly turned back by administration of *Pld1* cRNA (Figure 4D–F), implying PLD1 depletion may delay small vesicles fusing into large ones. Though vesicles changed in morphological characteristics, the protein levels of vesicle structural protein GOLGA2 and RAB11A were not altered in PLD1-depleted oocytes, as illustrated with western blot (Figure 5C [i-iii]). We also counted up Golgi apparatus-like clusters in per oocyte section, and found that the loss of PLD1 increased the number of Golgi-like clusters, which definitely indicates an inadequacy of Golgi apparatus fragmentation into vesicles as meiotic progression to metaphase (Figure 4G). At

---

immunofluorescence images showed PLD1 subcellular localization at GV, GVBD, MI, telophase I (tel I) and MII. Upon GVBD, PLD1 began to colocalize with the reassembled microtubules around chromosomes. Along with the cell cycle to MII, PLD1 overlapped with microtubules in the spindle apparatus. Arrowheads indicated dot-like aggregations of PLD1 in cytoplasm; arrows indicated PLD1 on spindle. Red, PLD1; green, acetylated-TUBA/α-tubulin (tubulin alpha); blue, DNA. Scale bar: 20 μm. (C) Representative immunofluorescence images illustrated PLD1 colocalization with vesicles in oocytes. Arrowheads indicated dot-like aggregations of PLD1 and GOLGA2 in cytoplasm. Red, PLD1; green, GOLGA2; blue, DNA. Scale bar: 20 μm.
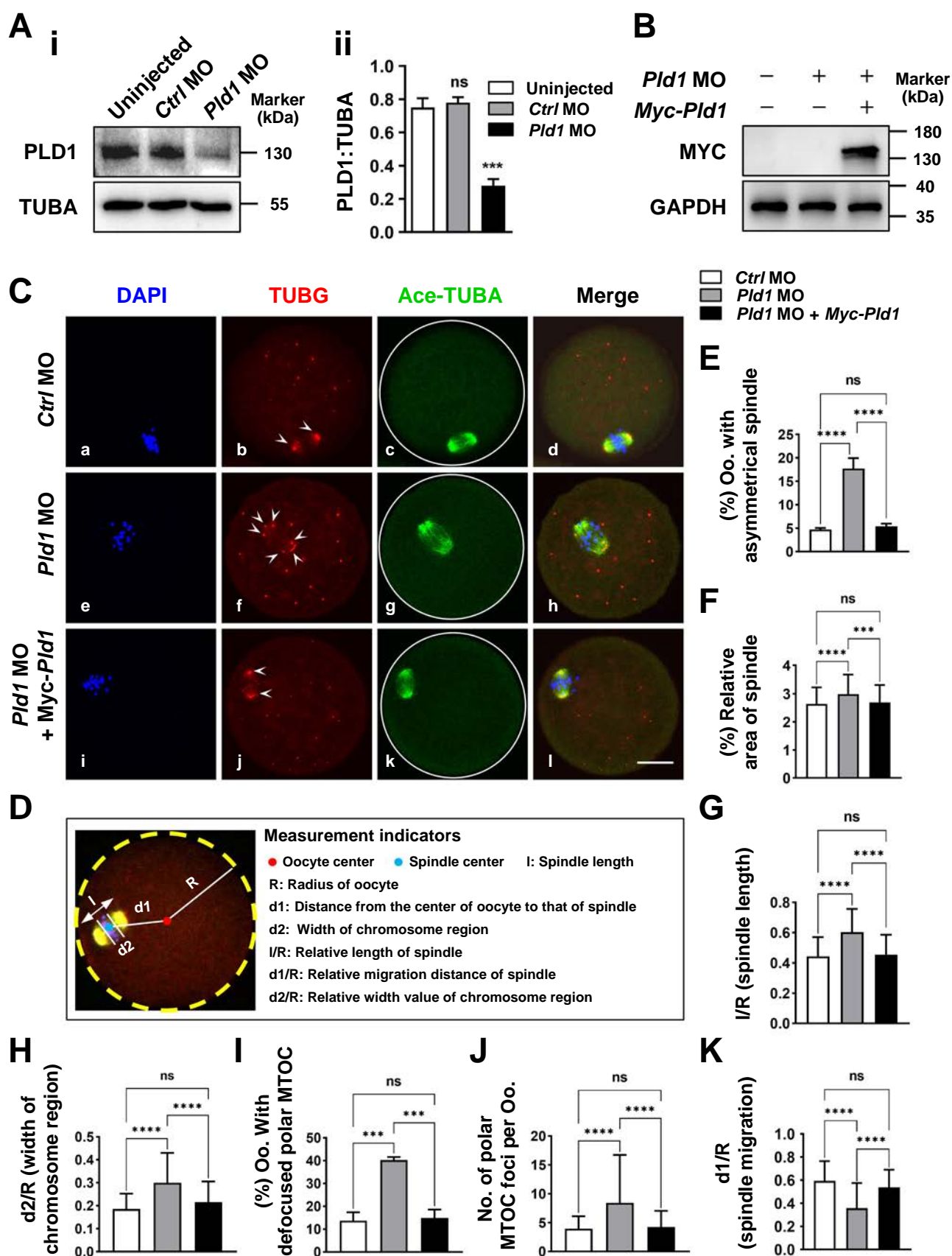
Figure 2. PLD1 depletion suppressed spindle migration and assembly in oocyte meiosis. (A-i) Western blot analysis of PLD1 protein in oocytes of the uninjected group, *Ctrl* MO group and *Pld1* MO group. Each sample had 90 oocytes. (A-ii) quantitative analysis of PLD1 protein level in oocytes of uninjected group, *Ctrl* MO group and *Pld1* MO group. (B) MYC protein level of oocytes with different microinjection treatments by western blot analysis. Each sample had 50 oocytes.

the same time, these Golgi-like clusters became swelling and irregular in shape, but such upregulating trend could be evidently rectified by co-microinjection of *Pld1* cRNA (Figure 4G–I). Therefore, the loss of PLD1 could destroy the fragmentation of Golgi apparatus and the dynamic fusion of vesicles.

In line with the results of *Pld1* MO, PLD1 inhibitor VU also decreased the proportion of large vesicles but increased that of the small ones in oocytes, and the changing trend became more and more apparent along with VU concentration increased from 5 μM to 10 μM, as demonstrated by immunofluorescence (Figure S3A–C). Furthermore TEM analysis confirmed similar changing trends in the quantity of vesicles, Golgi apparatus-like clusters, as well as abnormal-shaped clusters in oocytes treated with 5 μM VU (Figure S3D [c,d] and H). Together with the results of *Pld1* MO, it is reasonable to assume that PLD1 plays a essential role in Golgi apparatus fragmentation, vesicle morphogenesis and fusion in mouse oocyte meiosis.

PLD1 regulated F-actin density in mouse oocytes

Now that PLD1 suppression could impact vesicle assembly and fusion, so we continue to investigate whether the features of F-actin network was consequently affected. The MI oocytes were shortly incubated with molecular fluorescence probes Hoechst 33,342 and Cell mask green actin tracking stain, for labeling chromosomes and F-actin, then processed with live cell imaging. As showed in Figure 4J,K, in control oocytes, green signal of F-actin was mainly distributed beneath the cell membrane in a circular pattern, particularly some stronger fluorescence signal was congressed within a part of the circle just above the chromosome group, which actually represents the "actin cap". Generally, F-actin signal was faintly detected in the majority of cytoplasm area, only a few bright green filaments was labeled around the chromosomes in the cortical area. In contrast, *Pld1* MO treatment made dramatic difference, that is, a significantly enhancement of F-actin intensity was probed beneath the cell membrane and across the cytoplasmic area, with stronger F-actin signal around the chromosomes, which were not in the cortical area but near the center of the oocyte. In addition, there was no special "actin cap" along the cytomembrane. As expected, the elevated F-actin density could be significantly reversed by *Pld1* cRNA (Figure 4J [i-l]), logically consistent with cRNA's rectifying effects on vesicle morphology. Live cell imaging also confirmed enhanced intensity of F-actin by VU in a concentration-dependent manner (Figure S3I–J). Collectively, these data suggest that functional PLD1 actively participates in the regulation of F-actin assembly and stability, maybe through modulating vesicle fusion and dynamics.

VU inhibited vesicle re-assembly after BFA treatment

Brefeldin A (BFA) has been reported to affect the formation of recycling vesicles [8,35]. We assayed the effects of PLD1 inhibition on the features of vesicle disassembly and re-assembly during BFA administration and recovery after drug washout. As showed by immunofluorescence, the dot signal of vesicle protein GOLGA2 and RAB11A totally disappeared in oocytes cultured for 7 h with 20 μM BFA (Figure S4A [f-g]), these signals re-appeared as dot-like aggregations after the oocytes were washed out of BFA and recovered in fresh medium with DMSO for 1 h (Figure S4A [j-k]), in contrast, this reconstruction did not occur in the presence of VU (Figure S4A [n-o]). This result suggests that PLD1 maybe participate in the morphological construction of vesicles in mouse oocytes.

### Proximity in distance of PLD1 and vesicle proteins

To explore more about relationships between PLD1 and vesicle proteins, the interaction between PLD1 and GOLGA2 was firstly examined by duolink® proximity ligation assay (PLA) analysis. As showed in Figure 5A, intensive dot-like PLA signal was detected in positive control oocytes, which were incubated with antibodies to the known vesicle proteins GOLGA2 and RAB11A, while only few PLA signal was detected in negative control oocytes, administrated with only GOLGA2 antibody or PLD1 antibody. Same as positive control, bright PLA signal was found in oocytes incubated with PLD1 antibody and GOLGA2 antibody, but such incubation did not produce PLA signal when PLD1 was knocked down with MO. This indicates the proximity in distance of PLD1 and GOLGA2 in mouse oocytes. In agreement with PLA analysis, the immune-blots of both GOLGA2 and RAB11A were detected in oocyte lysate immunoprecipitated with PLD1 antibody instead of control IgG (Figure 5B). Together, these results imply a direct interaction between PLD1 and vesicle proteins in oocytes.

Both the regulatory and the catalytic region of PLD1 were required for its function in oocyte meiosis

To ensure the functional domain of PLD1 in charge for MTOC clustering and spindle migration in oocyte meiosis, we designed two mutants of PLD1, one is regulatorily inactive mutant PLD1^{F120A,R179Q}, the other is catalytically inactive mutant PLD1^{K898R}. Western blot analysis revealed that *Pld1*^{F120A,R179Q} and *Pld1*^{K898R} cRNA were both successfully expressed in oocytes (Figure 6A). Surprisingly, the overexpression of either mutant caused defocused MTOC, enlarged spindle, misaligned chromosomes and delayed spindle migration when compared to vehicle group

---

(C) Representative images of oocytes in *Ctrl* MO group, *Pld1* MO group and *Pld1* MO + *Myc-Pld1* group at 8 h of IVM. Arrowheads indicated dot-like congression of TUBG on spindle poles. Red, TUBG; green, acetylated-TUBA; blue, DNA. Scale bar: 20 μm. (D) computational method for measurement of spindle size and migration distance. (E-K) statistical analysis of oocytes with asymmetrical spindle (%), relative area of spindle (%), spindle length (l/R), width of chromosome region (d2/R), oocytes with defocused polar MTOC (%), numbers of polar MTOC foci per oocyte and spindle migration (d1/R) in *Ctrl* MO ($n = 116$), *Pld1* MO ($n = 137$) and *Pld1* MO + *Myc-Pld1* ($n = 120$) groups. All data were presented as the mean percentage (mean ± SEM) of at least three independent experiments. ***$p < 0.001$, ****$p < 0.0001$ by ordinary one-way ANOVA analysis.
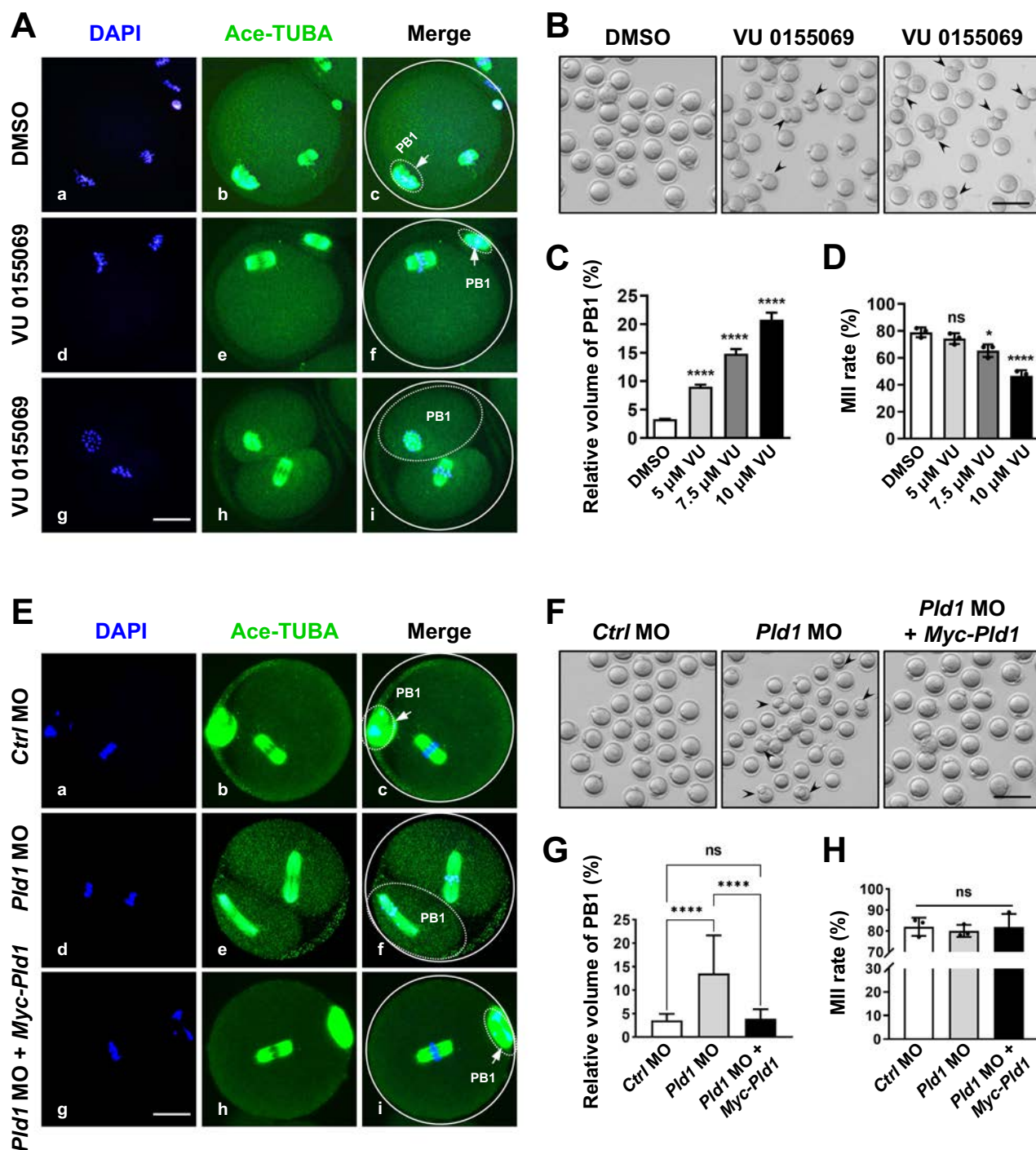
Figure 3. PLD1 modulated PB1 volume and asymmetric division in mouse oocytes. (A) Representative images of oocytes in DMSO group and VU groups at 16 h of IVM, respectively. Green, acetylated-TUBA; blue, DNA. Scale bar: 20 μm. (B) Representative images of oocytes in DMSO group and VU group at 16 h of IVM, respectively. Black arrows showed oocytes with large PB1. Scale bar: 400 μm. (C, D) statistical analysis of relative volumn of PB1(%) and MII rate (%) in DMSO group ($n = 146$) and 5 μM ($n = 149$), 7.5 μM ($n = 136$) and 10 μM ($n = 140$) VU-treated groups. (E) Representative images of oocytes in ctrl MO group, Pld1 MO group and Pld1 MO + myc-Pld1 group at 16 h of IVM, respectively. Green, acetylated-TUBA; blue, DNA. Scale bar: 20 μm. (F) Representative images of oocytes in ctrl MO group, Pld1 MO group and Pld1 MO + myc-Pld1 group at 16 h of IVM, respectively. Black arrows showed oocytes with large PB1. Scale bar: 400 μm. (G, H) statistical analysis of relative volumn of PB1(%) and MII rate (%) in ctrl MO group ($n = 128$), Pld1 MO group ($n = 120$) and Pld1 MO + myc-Pld1 group ($n = 114$). All data were presented as the mean percentage (mean ± SEM) of at least three independent experiments. ***$p < 0.05$, ****$p < 0.0001$ by ordinary one-way ANOVA analysis.

(Figure 6B–I). Furthermore, the extreme asymmetry of the first meiotic division was destroyed and the PB1 volume was increased (Figure 6J–L). However, neither of the mutants affected oocyte development to MII stage (Figure 6M). Thus both PLD1 regulatory activity and its catalytic activity is essential in MTOC clustering, spindle assembly and migration, as well as asymmetric division in oocytes.

Compared to vehicle group, the number of large vesicles was significantly decreased in MI oocytes of $Pld1^{F120A,R179Q}$ and $Pld1^{K898R}$ cRNA group, while that of small vesicles was increased, suggesting that both the regulatory and the catalytic
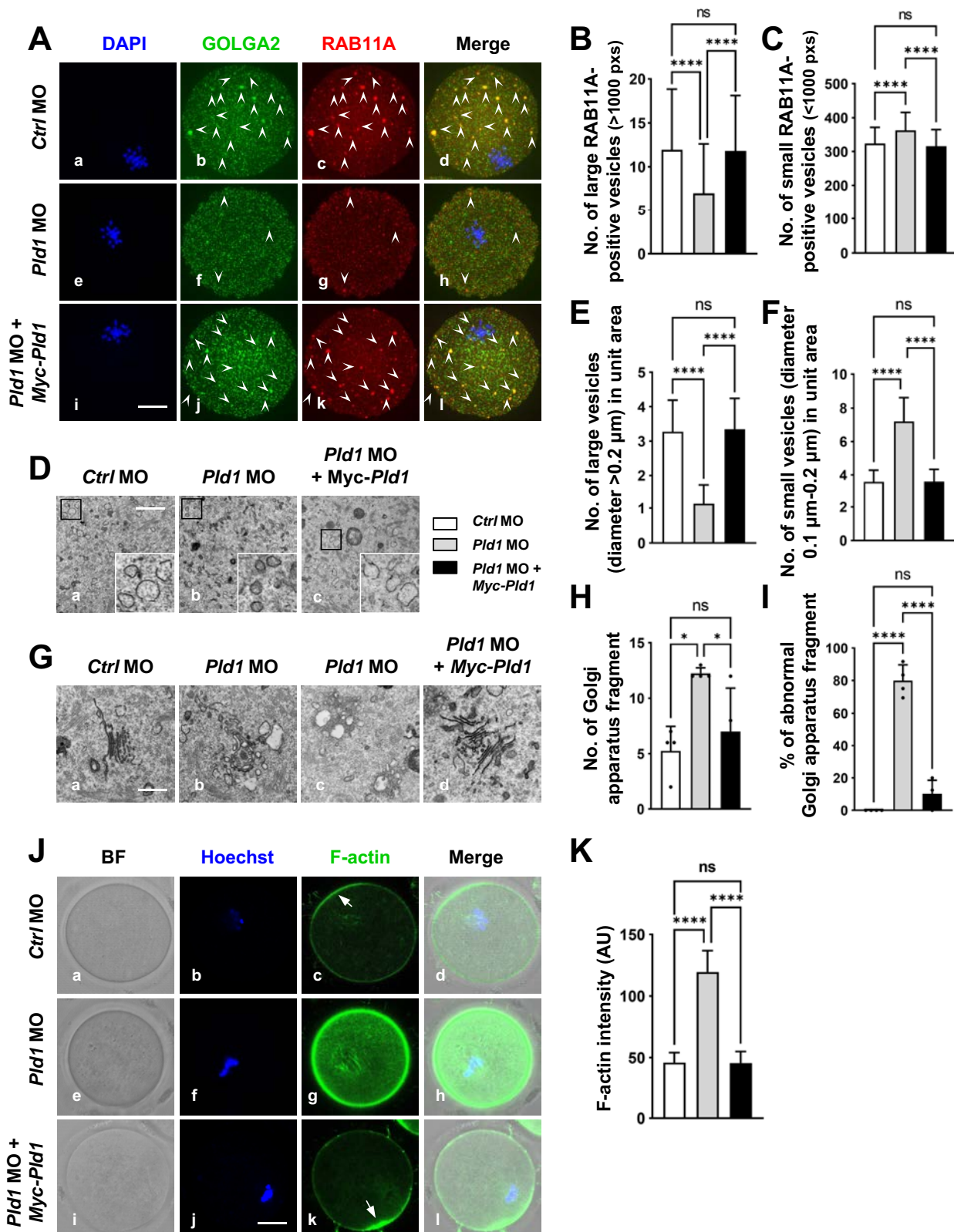
Figure 4. PLD1 depletion disturbed vesicle fusion and F-actin density in mouse oocytes. (A) Representative images of oocytes in *ctrl* MO group, *Pld1* MO group and *Pld1* MO + *myc-Pld1* group at 8 h of IVM, respectively. Arrowheads indicated patch-like aggregations of GOLGA2 and RAB11A in cytoplasm. Red, RAB11A; green, GOLGA2; blue, DNA. Scale bar: 20 μm. (B, C) statistical analysis of numbers of large RAB11A-positive vesicles (>1000 pixels) and small RAB11A-positive vesicles (<1000 pixels) in *ctrl* MO group (*n* = 112), *Pld1* MO group (*n* = 116) and *Pld1* MO + *myc-Pld1* group (*n* = 111). (D, G) Representative transmission electron microscopy (TEM) images of oocytes in *ctrl* MO group, *Pld1* MO group and *Pld1* MO + *myc-Pld1* group at 8 h of IVM, respectively. Scale bar: 500 nm. (E, F) statistical analysis of numbers of large vesicles (maximum diameter >0.2 μm) and small vesicles (maximum diameter 0.1 μm-0.2 μm) per 3 μm × 3 μm area in *ctrl* MO group (*n* = 4), *Pld1* MO group (*n* = 4) and *Pld1* MO + *myc-Pld1* group (*n* = 4). (H, I) statistical analysis of numbers of golgi apparatus fragment and percentage of abnormal golgi apparatus fragment (%) in *ctrl* MO group (*n* = 4), *Pld1* MO group (*n* = 4) and *Pld1* MO + *myc-Pld1* group (*n* = 4). (J) Representative images of oocytes in *ctrl* MO group, *Pld1* MO group and *Pld1* MO + *myc-Pld1* group at 8 h of IVM, respectively. Arrow indicated actin cap on cytoplasmic membrane. Green, F-actin; blue, DNA. Scale bar: 20 μm. (K) statistical analysis of F-actin fluorescence intensity (AU) in *ctrl* MO group (*n* = 40), *Pld1* MO group (*n* = 34) and *Pld1* MO + *myc-Pld1* group (*n* = 35). All data were presented as the mean percentage (mean ± SEM) of at least three independent experiments. ***$p < 0.05$, ****$p < 0.0001$ by ordinary one-way ANOVA analysis.
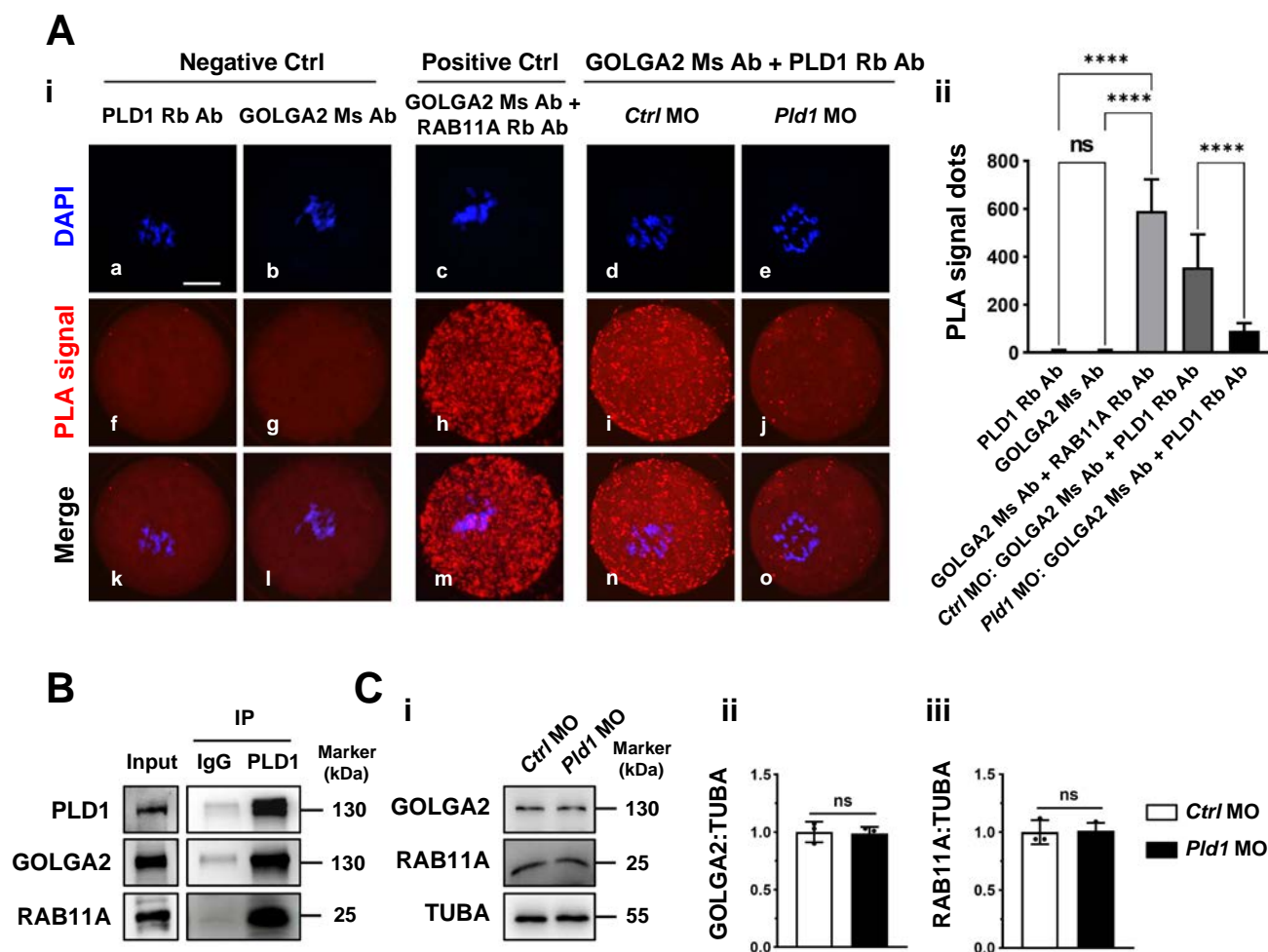
Figure 5. Direct physical interaction between PLD1 and vesicle proteins. (A-i) Representative images of PLA signals in different groups. PLA showed the proximity in distance of PLD1 and GOLGA2 in oocytes. Scale bar: 20 μm. (A-ii) quantitative analysis of PLA signal dots in different groups. >100 pixels dots were involved in the analysis. Data were presented as the mean percentage (mean ± SEM) of at least three independent experiments. PLD1 Rb ab group: $n = 100$; GOLGA2 ms ab group: $n = 100$; GOLGA2 ms ab + RAB11A Rb ab group: $n = 102$; Ctrl MO – GOLGA2 ms ab + PLD1 Rb ab group: $n = 107$; Pld1 MO – GOLGA2 ms ab + PLD1 Rb ab group: $n = 105$. (B) Co-IP was performed to determine the direct interaction between PLD1 and GOLGA2, RAB11A. Oocytes lysates were incubated with IgG or anti-PLD1 antibody, respectively. The blots of IP eluates were probed with anti-PLD1, anti-GOLGA2 and anti-RAB11A antibodies, respectively. (C-i) expression of GOLGA2 and RAB11A in oocytes in Ctrl MO group and Pld1 MO group by western blot. Each sample had 80 oocytes. (C-ii and iii) quantitative analysis of protein level changes in oocytes. All data were presented as the mean percentage (mean ± SEM) of at least three independent experiments. ***$p < 0.0001$ by ordinary one-way ANOVA analysis. $p > 0.05$ by unpaired t test.

region of PLD1 are involved in the dynamics of vesicle morphology (Figure 6N–P). Taken together, the regulatory and catalytic domains of PLD1 are both involved in the process of spindle assembly, vesicle transportation-mediated spindle migration, and thus asymmetric division in oocyte meiosis.

Blocking PLD1 decreased ACTR2, PtdIns(4,5)P$_2$ and p-CFL1 (Ser3) in oocytes

In order to further explore the molecular mechanism of PLD1 function in spindle assembly and cortical migration, the expression and distribution of some key molecules were investigated in oocytes with PLD1 loss, including PtdIns(4,5)P$_2$, CFL1, ACTR2, ACTR3 and FMN2, which are required for centrosome clustering, also F-actin assembly and vesicle fusion in somatic cells [7,12]. Compared to control MO group, the levels of PtdIns(4,5)P$_2$, p-CFL1 (Ser3) and

ACTR2 were apparently decreased in MI oocytes from the Pld1 MO group, but that of CFL1, ACTR3 and FMN2 remained unchanged, as illustrated by the western blot procedure (Figure 7A–H). Strickingly, the co-administration of Pld1 cRNA could effectively rescue the cellular levels of PtdIns(4,5)P$_2$, ACTR2 and p-CFL1 (Ser3) in PLD1-depleted oocytes (Figure 7I–L). Consistently, the immunofluorescence further confirmed that the number of large dots of ACTR2 (>1000 pixels) in cytoplasmic area were markedly reduced in Pld1 MO oocytes, and simultaneously the signal of either PtdIns(4,5)P$_2$ or p-CFL1 (Ser3) focusing on spindle poles was seriously diminished, and again, all these local distribution defects could be recouped by Pld1 cRNA (Figure 7M–S). In line with Pld1 MO results, VU also dose-dependently decreased PtdIns(4,5)P$_2$, p-CFL1 (Ser3) and ACTR2 in oocytes, as demonstrated with both western blot (Figure S5A) and immunofluorescence (Figure S5B–H). In addition,
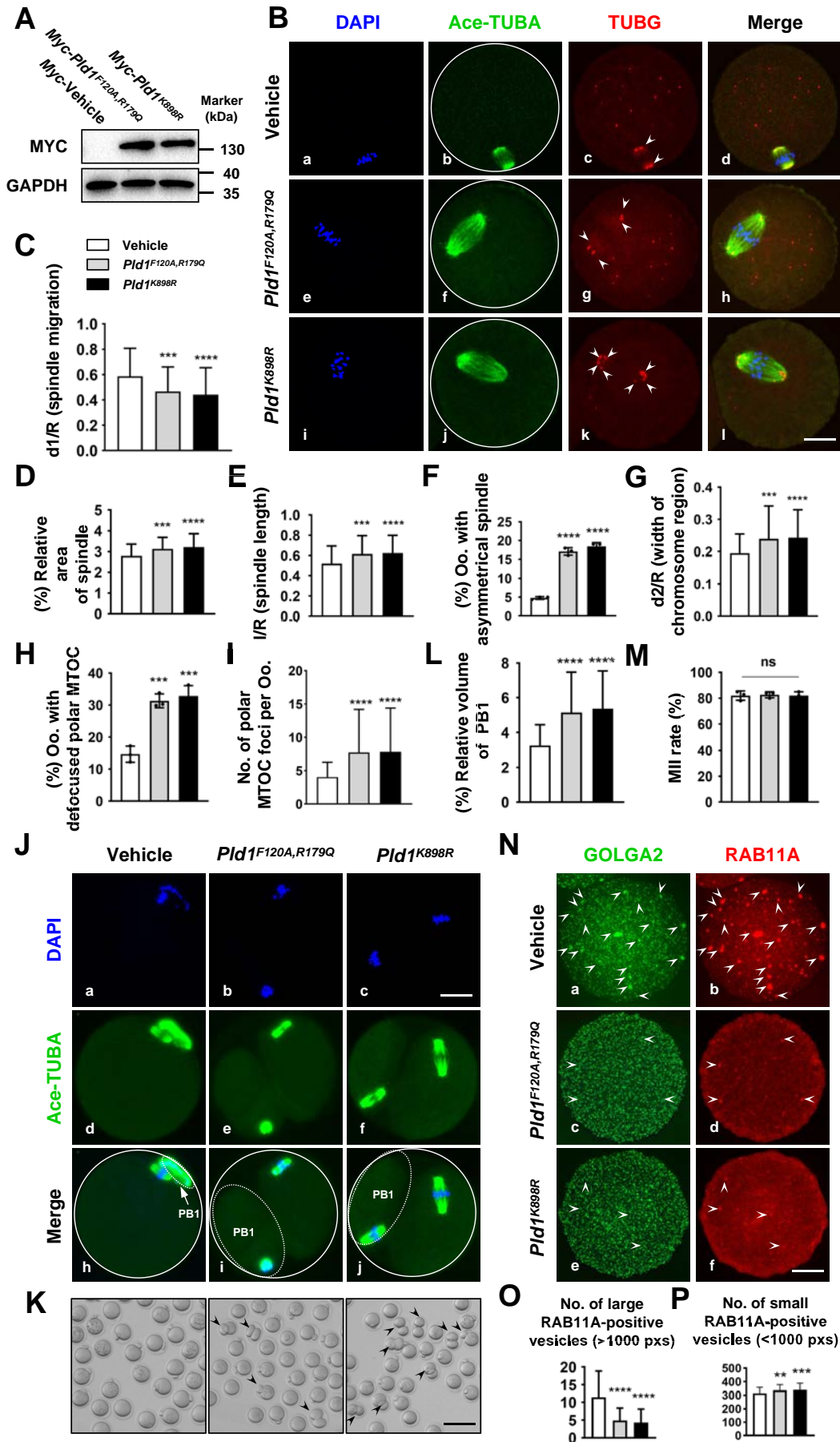
Figure 6. Both regulatory and catalytic region of PLD1 were required in spindle assembly and migration. (A) MYC-protein level of oocytes with vehicle, *Pld1^{F120A,R179Q}* and *Pld1^{K898R}* cRNA microinjection treatments by western blot analysis. Each sample had 50 oocytes. (B) Representative images of MI oocytes in vehicle, *Pld1^{F120A,R179Q}*

the blots of PtdIns(4,5)P$_2$, ACTR2 and CFL1 were positively present in the cell lysate preincubated with PLD1 antibody instead of control IgG, indicating direct physical interactions of these molecules with PLD1 (Figure 7T). Collectively, PLD1 actively functions to maintain the rational levels of PtdIns(4,5)P$_2$, p-CFL1 (Ser3) and ACTR2 in oocytes, thus regulating MTOC clustering and spindle migration.

CFL1^{S3E} rectified the defects in MTOC clustering and spindle assembly in PLD1-depleted oocytes

CFL1 is related to centrosome integrity and function [12], and here we found the blocking of PLD1 destroyed the expression and location of p-CFL1 (Ser3) in oocytes. We further investigated whether this change is responsible for the alterations in MTOC and spindle, as well as chromosomes alignment. We constructed CFL1^{S3A}, which does not undergo phosphorylation, and CFL1^{S3E}, the pseudo-phosphorylated form. The in vitro produced cRNA of both Cfl1^{S3A} and Cfl1^{S3E} was successfully expressed in oocytes, as illustrated by the western blot (Figure 8A). Immunofluorescence showed that Cfl1^{S3A} cRNA definitely brought about defocused MTOCs, enlarged and center-positioned spindles with misaligned chromosomes in MI oocytes, exactly the same as the phenotype induced by Pld1 MO. In contrast, the co-injection of Cfl1^{S3E} cRNA could significantly rescue some phenotypes in PLD1-depleted oocytes, including MTOC defocusing, spindle largening and chromosome misalignment, but excluding spindle migration failure (Figure 8B–I). These results suggest that PLD1 function in maintaining the morphology of MTOC and spindle is mediated by CFL1, at least partially. Interestingly, the down-regulated CFL1 phosphorylation may be not in charge for the spindle migration failure in PLD1-depleted oocytes.

Exogenous PtdIns(4,5)P$_2$ relieved PLD1-inhibition induced defects in MTOC clustering and spindle assembly

Previous evidences illustrate that PtdIns(4,5)P$_2$ is an upstream regulatory molecule of actin which capable of promoting actin polymerization, and also a partner of p-CFL1 (Ser3) in a polar complex which regulates centrosome integrity in several cell types [12,13]. We found here that the level and polar concentration of PtdIns(4,5)P$_2$ was reduced in oocytes treated with VU or Pld1 MO. Therefore, we continue to explore whether the reduction of PtdIns(4,5)P$_2$ is the direct driving factor for the abnormal changes caused by PLD1 inhibition with VU. As demonstrated by immunofluorescence, the application of exogenous PtdIns(4,5)P$_2$ could dramatically correct the alterations in MTOC focusing, spindle size and chromosomes

alignment, but not the delay in spindle migration (Figure 8J–Q, Figure S6), indicating that PLD1 promotes the setup and maintenance of MTOC polar focusing and spindle morphology in oocytes through maintaining a rational level of PtdIns(4,5)P$_2$, at least partially, but which is not essential for spindle migration.

ACTR2 overexpression reversed PLD1-depletion induced alterations in MTOC clustering and spindle migration

The ACTR2-ACTR3 complex is required in vesicle trafficking in enterocytes [36], so it's necessary to verify whether ACTR2 reduction is one of the implementation factors causing specific changes in oocytes with absence of PLD1 function. As illustrated by western blot, the in vitro produced Actr2 cRNA could be successfully translated in mouse oocytes (Figure 9A), and its expression apparently rectified all the abnormal changes induced by PLD1 depletion. Not only the morphological changes in MTOC and spindle but also the delayed migration of spindle were perfectly redressed in MI oocytes (Figure 9B [a-l], C-I), recovering the ultra asymmetry of cytokinesis and the minimum size of PB1 in MII oocytes (Figure 9B [m-x], 9J). What's more, Actr2 cRNA could substantially rescue vesicle morphology change induced by Pld1 MO (Figure 9K–M), this explains, to some extent, the mechanism by which overexpressed ACTR2 regulates spindle migration. In summary, these results indicate that PLD1 presverves a rational level of ACTR2, also including at least PtdIns(4,5)P$_2$ and p-CFL1 (Ser3), so as to promote MTOC clustering and spindle migration in oocyte meiosis.

No rectifying effect of WASL 388–501 on spindle assembly and migration in PLD1-depleted oocytes

As reported, WASL/N-WASP (WASP like actin nucleation promoting factor) can activate the ACTR2-ACTR3 complex to stimulate actin polymerization [37], so we further investigate whether WASL works at the downstream of PLD1 in regulating MTOC and spindle by activating ACTR2. We found that the protein levels of WASL and its phosphorylation forms p-WASL (Tyr256) and p-WASL (Ser484, Ser485) were all decreased in Pld1-MO-injected oocytes compared to the control cells, confirming WASL is a downstream target of PLD1 (Figure S7A-D). It is said that the full-length WASL is only weakly active in function, and the C-terminal fragment of WASL strongly accelerates ACTR2-ACTR3-mediated actin assembly, confers a dramatic 30-fold acceleration [37]. Though the cRNA of constructed C-terminal fragment of WASL (Wasl 388–501) was efficiently translated in mouse

and Pld1^{K898R} groups, respectively. Arrowheads indicated signal of TUBG on spindle poles. Red, TUBG; green, acetylated-TUBA; blue, DNA. Scale bar: 20 µm. (C-I) statistical analysis of spindle migration (d1/R), relative area of spindle (%), spindle length (l/R), asymmetrical spindle (%), width of chromosome region (d2/R), oocytes with defocused polar MTOC (%) and polar MTOC foci per oocyte in vehicle (n = 113), Pld1^{F120A,R179Q} (n = 102) and Pld1^{K898R} (n = 101) groups. (J) Representative images of MII oocytes in vehicle, Pld1^{F120A,R179Q} and Pld1^{K898R} groups, respectively. Green, acetylated-TUBA; blue, DNA. Scale bar: 20 µm. (K) Representative images of MII oocytes in vehicle, Pld1^{F120A,R179Q} and Pld1^{K898R} groups, respectively. Black arrows showed oocytes with large PB1. Scale bar: 400 µm. (L, M) statistical analysis of relative volumn of PB1(%) and MII rate (%) in vehicle (n = 100), Pld1^{F120A,R179Q} (n = 103) and Pld1^{K898R} (n = 102) groups. (N) Representative images of MI oocytes in vehicle, Pld1^{F120A,R179Q} and Pld1^{K898R} groups, respectively. Arrowheads indicated patch-like aggregations of GOLGA2 and RAB11A in cytoplasm. Red, RAB11A; green, GOLGA2. Scale bar: 20 µm. (O, P) statistical analysis of numbers of large RAB11A-positive vesicles (>1000 pixels) and small RAB11A-positive vesicles (<1000 pixels) in vehicle (n = 115), Pld1^{F120A,R179Q} (n = 105) and Pld1^{K898R} (n = 110) groups. All data were presented as the mean percentage (mean ± SEM) of at least three independent experiments. ***p < 0.001, ****p < 0.0001 by ordinary one-way ANOVA analysis.
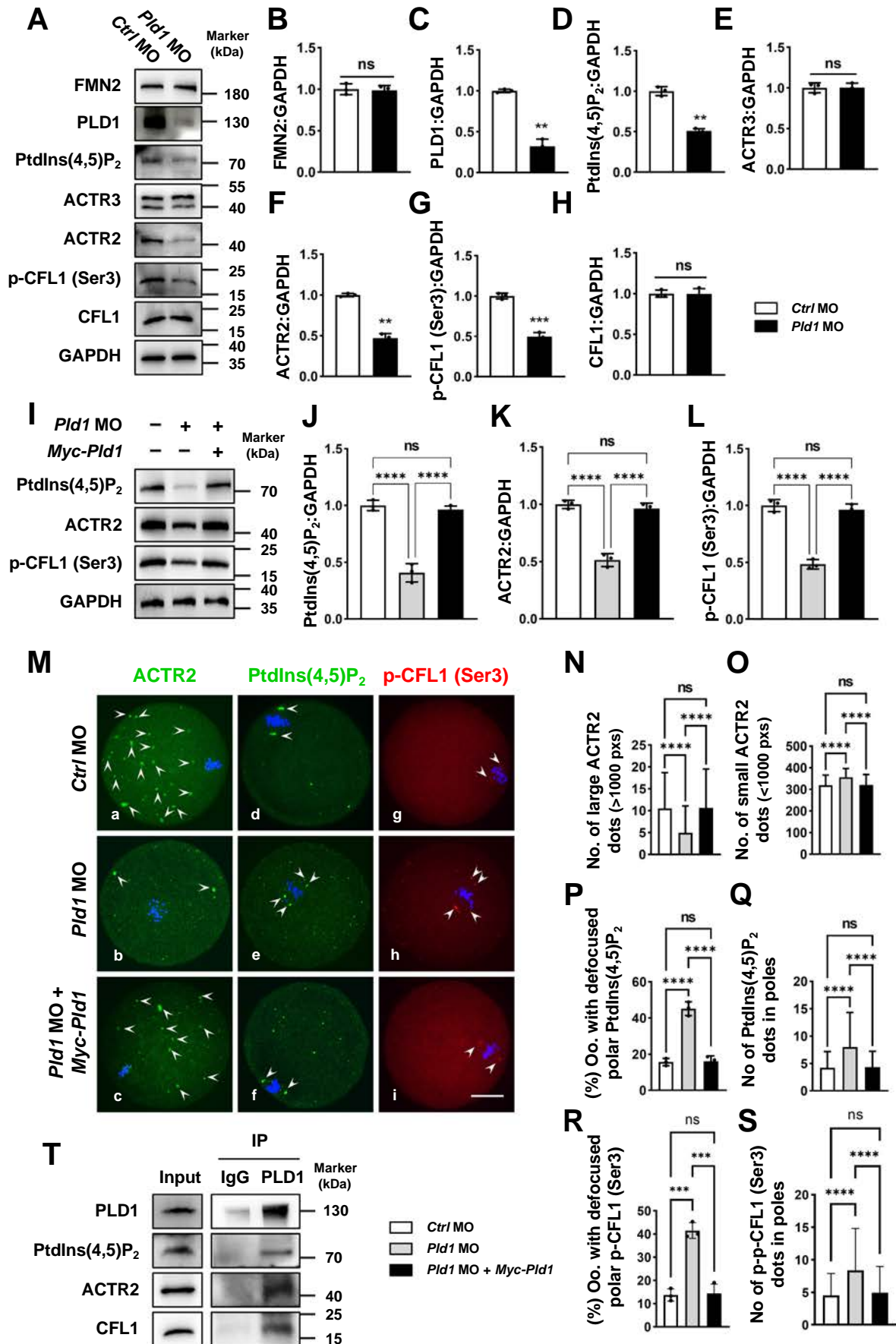
Figure 7. PLD1 depletion decreased PtdIns(4,5)P2, p-CFL1(Ser3) and ACTR2. (A) changes of protein expression in oocytes in *ctrl* MO group and *Pld1* MO group by western blot. The blots were incubated with anti-FMN2, anti-PLD1, anti-PtdIns(4,5)P$_2$, anti-ACTR3, anti-ACTR2, anti-CFL1, anti-p-CFL1(Ser3) and anti-GAPDH antibodies, respectively. Each sample had 90 oocytes. (B – H) quantitative analysis of protein level changes in oocytes. (I) changes of protein expression in oocytes

oocytes, but this did not rescue ACTR2 level in PLD1-depleted oocytes, accordingly bringing about no positive recovery in MTOC and spindle (Figure S7E–M). This result indicates the effects of ACTR2 mediating PLD1 function is independent of WASL.

PLD1 depletion enhanced autophagy

PLD1 has been proved to regulate autophagy and associated with centrosome integrity [12,29–32]. Using transmission electron microscopy (TEM), we found the number of autophagosomes and autolysosomes in unite section was significantly higher in VU-treated oocytes than control cells (Figure S8A). Increased formation of autophagosomes and autolysosomes were also found in *Pld1*-MO-treated oocytes, and importantly, this upregulation could be redressed dramatically by exogenous *Pld1* cRNA microinjection (Figure 10A,B). In addition, the protein levels of MTOR and RPS6KB1/S6K1 (ribosomal protein S6 kinase B1) were stable, while p-MTOR (S2448) , p-RPS6KB (T389) and SQSTM1/p62 (sequestosome 1) were decreased, and instead MAP1LC3B/LC3-II (microtubule-associated protein 1 light chain 3 beta), BECN1/Beclin 1 and ATG5 (autophagy related 5) were increased in the *Pld1* MO group (Figure 10C), verifying PLD1 depletion can enhance autophagy activity. Actually, there is direct physical interaction between PLD1 and autophagy protein SQSTM1 and LC3, as illustrated by immunoprecipitation, that is SQSTM1 and LC3 were explicitly present in the cell lysate preincubated with PLD1 antibody but not control IgG (Figure 10D). The defocused MTOC and delayed spindle migration were also observed in oocytes treated with autophagy activator rapamycin or adezmapimod (Figure S9), suggesting the enhanced autophagic flux may account for the abnormalities in the absence of PLD1 activity.

Therefore, it may be reasonable to assume that the blocking of PLD1 upregulates the degradation of $PtdIns(4,5)P_2$, ACTR2 and p-CFL1 (Ser3) through enhancing autophagy flux. As demonstrated by western blot in mouse oocytes, the total amount of UB (ubiquitin) was apparently decreased by *Pld1* MO, but could be reversed by co-administration of autophagy inhibitor bafilomycin A_1 (Baf-A1) (Figure S8B), thus preliminarily suggesting PLD1 blocking can enhance autophagy-mediated protein degradation. As expected, Baf-A1 dramatically enhanced the levels of $PtdIns(4,5)P_2$, ACTR2 and p-CFL1 (Ser3) in comparion with DMSO treatment, and even blocked the decreasing of these molecules in oocytes treated with *Pld1* MO (Figure 10E–J), fully vertifying that the loss of PLD1 fires up autophagic degradation of $PtdIns(4,5)P_2$, ACTR2 and p-CFL1 (Ser3). Interestingly, we found the autophagic protein SQSTM1 and LC3-II were asymmetrically distributed in oocyte cytoplasm, specially the dot-like signal was absent in the area where suggestively the spindle exists. Baf-A1 only changes the dote size of SQSTM1 and LC3-II, but not their asymmetric distribution pattern. In contrast, *Pld1* MO destroyed not only the aggregation size of SQSTM1 and LC3-II, but also their specific regional distribution, causing uniformly spreading of small signal dots across the cytoplasm, however, these changes could be rescued by co-application of Baf-A1 (Figure 10K–L). The results above suggest that PLD1 modulates autophagy in mouse oocytes in a region-specific manner, the blocking of PLD1 could enhance autophagy and subsequently the degradation of $PtdIns(4,5)P_2$, ACTR2 and p-CFL1 (Ser3).

Autophagy inhibition rescued spindle assembly and migration in PLD1-depleted oocytes

Next, we investigated whether autophagy inhibition could rectify the defects related to MTOC and spindle. Baf-A1 did not exert apparent influence on MTOC and spindle in oocytes from *Ctrl* MO group (Figure 11A [a-h], B-H), but brought into play positive correction effect in *Pld1* MO group, specifically, all the alterations in MTOC clustering, spindle size and migration, were substantially rescued (Figure 11A [i-p], B-H). Additionally, the other two autophagy inhibitors, MHY1485 and wortmannin, produced similar rectifying effects in oocytes with PLD1 knockdown with MO (Figure S10). This suggests that the hyperfunctioning autophagy may be the basic reason for impaired features of MTOC and spindle in oocytes after PLD1 knockdown.

Further immunofluorescence showed that the proportion of large vesicles was significantly increased in oocytes of Baf-A1 treatment group than control, companied with a decrease in small vesicles. This pattern was opposite to the *Pld1* MO group, in which the number of large vesicles decreased while that of small ones increased (Figure 11I [a-h], J-K). However, the co-administration of Baf-A1 could obviously reverse the vesicle composition pattern in *Pld1* MO group, increasing the population of large vesicle (Figure 11I [i-p], J-K). In addition, the treatment with Baf-A1 alone significantly weakened the fluorescence intensity of F-actin network in oocytes (Figure 11L [a-h], M), and as expected, co-application of this drug could apparently down-regulate the enhanced F-actin fluorescence intensity caused by *Pld1* MO (Figure 11L [i-p], M). Together, it is safe to say that PLD1 promotes spindle assembly and vesicle-mediated migration by suppressing autophagy activity.

in groups of *ctrl* MO, *Pld1* MO and *Pld1* MO + *myc-Pld1* by western blot. The blots were incubated with anti-PtdIns(4,5)P_2, anti-ACTR2, anti-p-CFL1 (Ser3) and anti-GAPDH antibodies, respectively. Each sample had 90 oocytes. (J-L) quantitative analysis of protein level changes in oocytes. (M) Representative images of MI oocytes in *ctrl* MO, *Pld1* MO and *Pld1* MO+ *myc-Pld1* groups. Arrowheads indicated foci of signal of ACTR2 and PtdIns(4,5)P_2. Red, p-CFL1 (Ser3); green, ACTR2 or PtdIns(4,5)P_2; blue, DNA. Scale bar: 20 μm. (N, O) statistical analysis of numbers of large ACTR2 dots (>1000 pixels) and small ACTR2 dots (<1000 pixels) in groups of *ctrl* MO (n = 102), *Pld1* MO (n = 99) and *Pld1* MO + *myc-Pld1* (n = 102) groups. (P, Q) statistical analysis of oocytes with defocused PtdIns(4,5)P_2 (%) and numbers of PtdIns(4,5)P_2 dots in poles in groups of *ctrl* MO (n = 102), *Pld1* MO (n = 99) and *Pld1* MO + *myc-Pld1* (n = 102). (R, S) statistical analysis of oocytes with defocused polar p-CFL1 (Ser3) (%) and numbers of p-CFL1 (Ser3) dots in poles in groups of *ctrl* MO (n = 102), *Pld1* MO (n = 99) and *Pld1* MO + *myc-Pld1* (n = 102). (T) Co-IP was performed to determine the interaction between PLD1 and PtdIns(4,5)P_2, ACTR2 and CFL1. Oocytes lysates were incubated with IgG or anti-PLD1 antibody. The blots of IP eluates were probed with anti-PLD1, anti-PtdIns(4,5)P_2, anti-ACTR2 and anti-CFL1 antibodies, respectively. All data were presented as the mean percentage (mean ± SEM) of at least three independent experiments. ***p < 0.01, ****p < 0.001,****p < 0.0001 by unpaired t test or ordinary one-way ANOVA analysis.
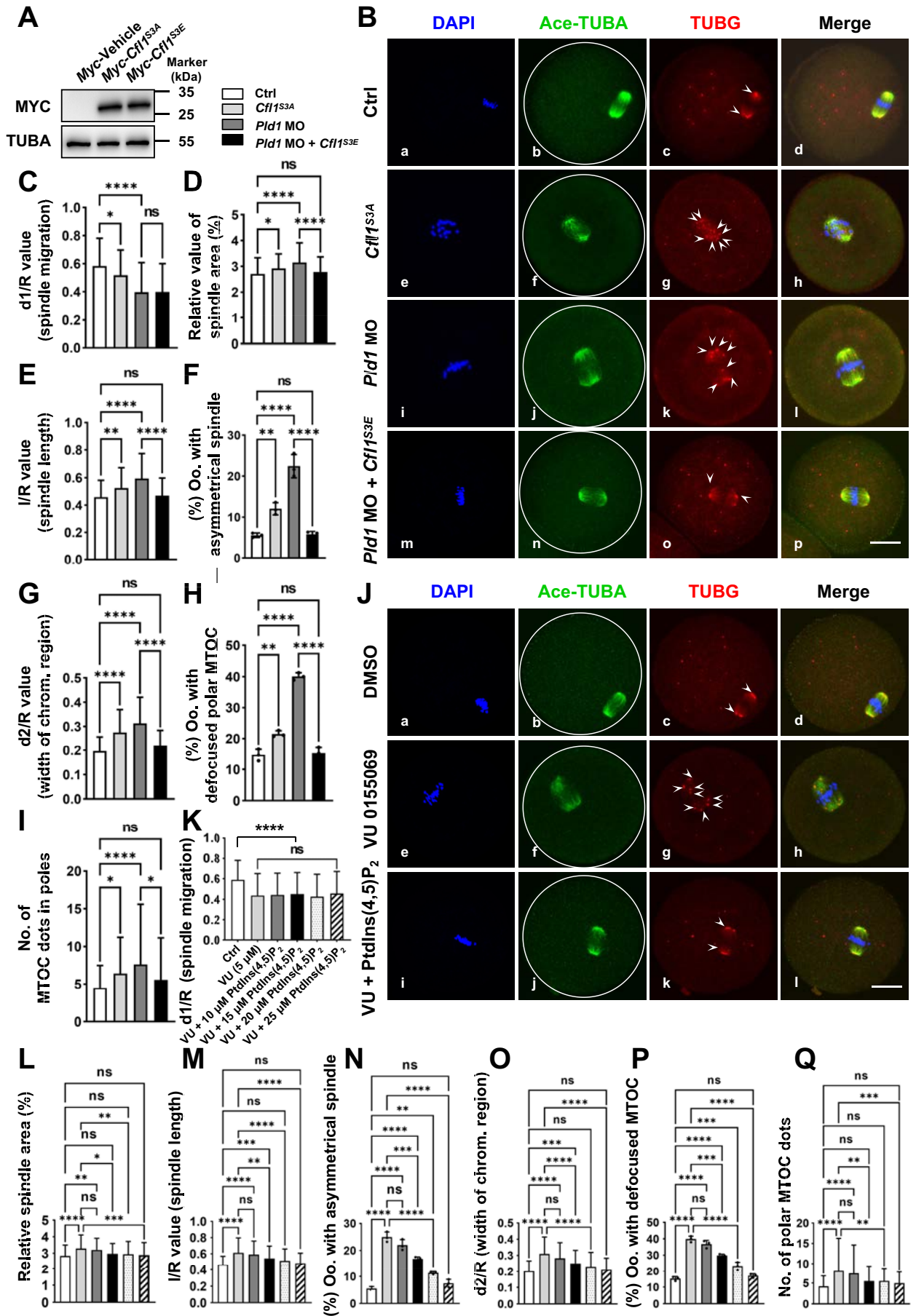
Figure 8. CFL1^{S3E} and exogenous PtdIns(4,5)P2 can rescue MTOC fragmentation caused by PLD1 depletion or inhibition. (A) Western blot analysis of MYC-protein level in oocytes injected with vehicle, *Cfl1^{S3A}* and *Cfl1^{S3E}* cRNA. Each sample contained 50 oocytes. (B) Representative images of MI oocytes in groups of *Ctrl*, *Cfl1^{S3A}*, *Pld1* MO and *Pld1* MO + *Cfl1^{S3E}*, respectively. Arrowheads indicated signal of TUBG on spindle poles. Red, TUBG; green, acetylated-TUBA; blue, DNA. Scale bar: 20 μm.

Discussion

In this study, we found that PLD1 is highly expressed at every meiotic stage and has multisite locations on spindle, RAB11A-positive vesicles and autophagic vacuoles in mouse oocytes. Chemical or genetic blocking of PLD1 dramatically disturbed MTOC clustering, spindle assembly and cortical migration by decreasing cellular levels of ACTR2, PtdIns(4,5)P_2 and p-CFL1 (Ser3) in a manner of enhancing autophagy flux (Figure 12).

Spindle migration is powered by F-actin network dynamics. FMN2 and the ACTR2-ACTR3 complex, separately work as "straight" and "branched" actin nucleators, which are recruited on RAB11A-positive vesicles, and thereby the active fission and fusion processes of vesicles trigger the mobility of F-actin network [3,4,8]. Specially, vesicles move and mutually integrate along the tracks of "branched" F-actin nucleated by ACTR2, and the loss of functional ACTR2-ACTR3 complex negatively affects vesicle trafficking and fusing [36]. In our study, we found there is a direct physical interaction between PLD1 and ACTR2 in mouse oocytes, and PLD1 depletion only decreased the expression of ACTR2, but not ACTR3 or FMN2. The overexpression of ACTR2 could perfectly rescue the abnormal phenotypes induced by PLD1 depletion, especially the alterations in vesicle structures and fusion, cytoplasmic F-actin density and spindle migration. So PLD1 is a vesicle-associated protein, and ACTR2 may work as the mediator of PLD1 function in regulating vesicle fusion and spindle cortical migration in mouse oocyte meiosis.

In oocyte meiosis, finely-regulated MTOC fusion and clustering on spindle poles is very important for bipolar spindle formation and maintenance [10]. CFL1 is originally known for its function to severe actin filaments, its activity is negatively regulated by phosphorylation on Ser3 by LIMK1 (LIM domain kinase 1) [38]. Recently, phospho-CFL1 is proved to promote centrosome integrity in human osteosarcoma cell line [12]. PtdIns(4,5)P_2 facilitates p-CFL1 (Ser3) focusing on spindle poles, and the loss of PtdIns(4,5)P_2 damages polar localization of p-CFL1 (Ser3), causing disruption of centrosome integrity in somatic cells [12,13]. To our knowledge, there are still no published data about the function of PtdIns(4,5)P_2 or CFL1 in spindle assembly and maintenance in oocyte meiosis.

Here we found that PtdIns(4,5)P_2 and p-CFL1 (Ser3) were colocalized with MTOC key component TUBG on spindle poles in mouse oocytes, and the expression of $Cfl1^{S3A}$ cRNA, the un-phosphorylable mutant, could severely break MTOC clustering, causing the formation of large spindle. Similar changes also occured in oocytes with PLD1 blocking, in which the general level and polar location of p-CFL1 (Ser3) and PtdIns(4,5)P_2 were apparently diminished, however,

these morphological changes could be intriguingly reversed by exogenous $Cfl1^{S3E}$ cRNA, the pseudo-phosphorylated mutant of CFL1, and also rectified by application of exogenous PtdIns(4,5)P_2. Therefore phospho-CFL1 and PtdIns(4,5)P_2 are truly required for the morphological shaping of MTOC and spindle in oocytes, consistent with their function in maintaining somatic centrosome integrity [12,13]. Though CFL1 and PtdIns(4,5)P_2 have mainly been established as central regulators of the actin cytoskeleton [25,26], the re-introduction of PtdIns(4,5)P_2 or CFL1^{S3E} only exhibited remedial effects on MTOC and spindle structure, but not on spindle migration, a process drived by F-actin mobility in the cytoplasm. This may suggest the function of PtdIns(4,5)P_2 or p-CFL1 (Ser3) has spatiotemporal specificity, particularly in mitotic or meiotic division, during which time these two molecules dominantly gather on spindle poles and may contribute to forming a complex to promote the integrity of centrosome or acentriolar MTOC, possibly just regulating F-actin dynamics at the local area of spindle poles.

Typically, the enzymatic activity of PLD1 catalyzes the synthesis of phosphatidic acid, which sequently activates PIP-5 kinase, evoking an increase in PtdIns(4,5)P_2 synthesis [27]. Recently, PLD1 is proved to promote CFL1 phosphorylation/inactivation and inhibit CFL1-mediated mitochondrial toxicity in brain neurons [39]. Consistent with these information, we found both PtdIns(4,5)P_2 and p-CFL1 (Ser3) has direct physical interaction with PLD1, their expression was reduced in PLD1-blocked oocytes and could be efficiently recovered by the overexpression of $Pld1$ cRNA, thereby PLD1 must work to preserve PtdIns(4,5)P_2 and p-CFL1 (Ser3) in rational level, so to facilitate the setup and maintenance of a functional complex essential for MTOC clustering.

It has been proved that the ACTR2-ACTR3 complex localizes to the centrosome in several somatic cells, with an inherent role in activating centrosomal enzyme AURKA (aurora kinase A) and nucleating F-actin, thereby promotes the proper mitotic spindle formation and chromosome congression [40–42]. In agreement with this, we found ACTR2 is also required for the orderly shaping of MTOC and spindle in oocytes, besides its role in spindle migrating. ACTR2 was labeled across the spindle apparatus when oocytes were fixed in a different procedure (data not showed), and the salvage of ACTR2 diminution by exogenous $Actr2$ cRNA could ideally improve the morphology of MTOC and spindle in PLD1-suppressed oocytes. So in sum, PLD1 promotes MTOC clustering and spindle assembly through maintaining reasonable levels of PtdIns(4,5)P_2, p-CFL1 (Ser3) and ACTR2 in oocytes.

(C-I) statistical analysis of spindle migration (d1/R), relative area of spindle (%), spindle length (l/R), oocytes with asymmetrical spindle (%), width of chromosome region (d2/R), defocused polar MTOC (%) and polar MTOC foci per oocyte in groups of ctrl ($n = 125$), $Cfl1^{S3A}$ ($n = 123$), Pld1 MO ($n = 124$) and Pld1 MO + $Cfl1^{S3E}$ ($n = 129$). (J) Representative images of MI oocytes in DMSO, 5 μM VU and VU + PtdIns(4,5)P_2 groups. Arrowheads indicated signal of TUBG on spindle poles. Red, TUBG; green, acetylated-TUBA; blue, DNA. Scale bar: 20 μm. (K-Q) statistical analysis of spindle migration (d1/R), relative area of spindle (%), spindle length (l/R), width of chromosome region (d2/R), oocytes with asymmetrical spindle (%), defocused polar MTOC (%) and polar MTOC foci per oocyte in different groups. DMSO group: $n = 120$, 5 μM VU group: $n = 114$, VU +10 μM PtdIns(4,5)P_2 group: $n = 118$, VU +15 μM PtdIns(4,5)P_2 group: $n = 116$, VU +20 μM PtdIns(4,5)P_2 group: $n = 121$, VU +25 μM PtdIns(4,5)P_2 group: $n = 118$. All data were presented as the mean percentage (mean ± SEM) of at least three independent experiments. ***$p < 0.05$, ****$p < 0.01$, ****$p < 0.001$,***$p < 0.0001$ by ordinary one-way ANOVA analysis.
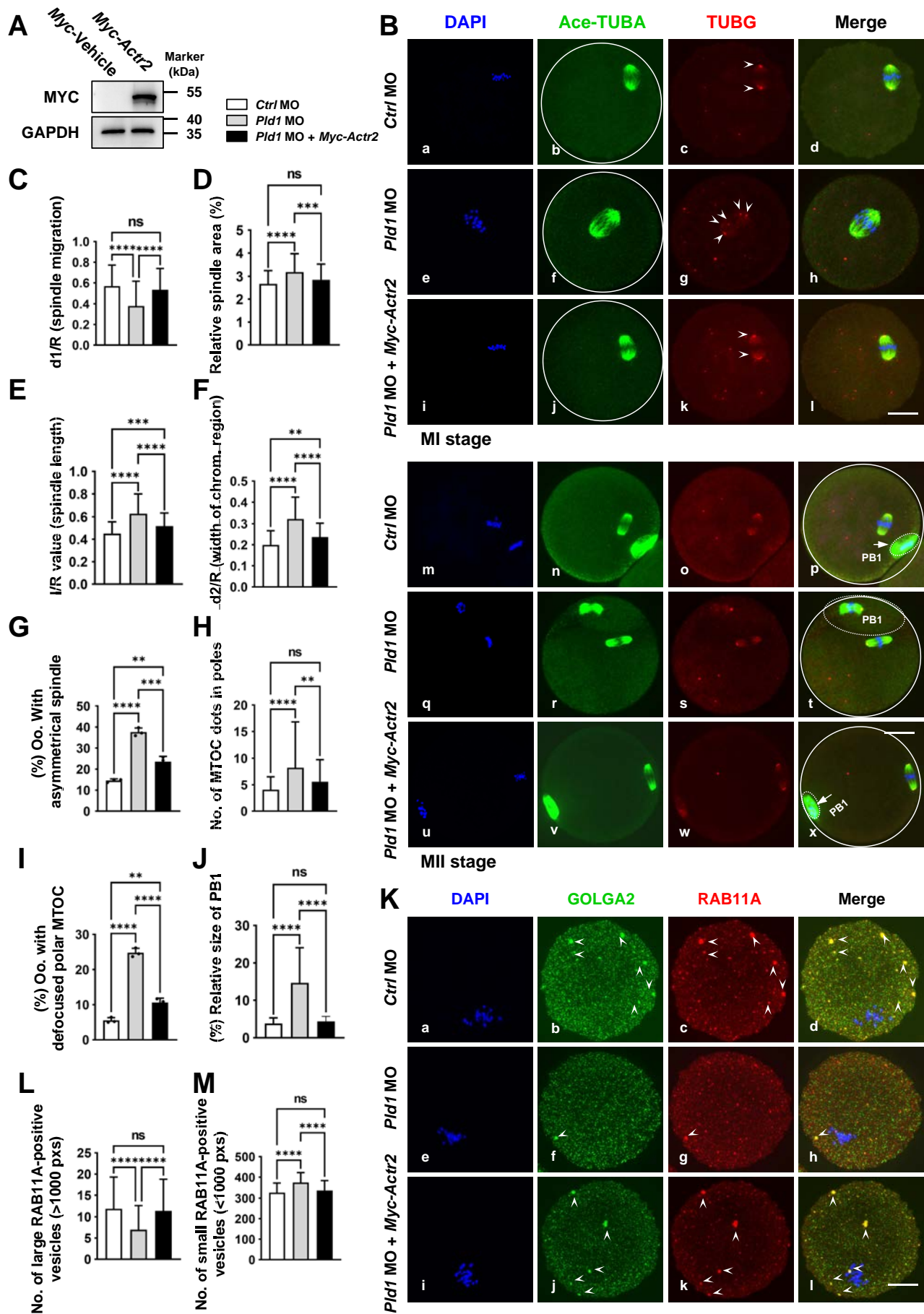
Figure 9. ACTR2 overexpression reversed the failures in MTOC focusing, spindle assembly and migration in PLD1-depleted oocytes. (A) MYC-protein level in oocytes injected with vehicle and *myc-Actr2* cRNA by western blot analysis. Each sample had 50 oocytes. (B) Representative images of MI oocytes in groups of *ctrl* MO, *Pld1*

We detected increased formation of autophagosome and auto-lysosome in PLD1-suppressed oocytes, with characteristic changes in LC3-II, SQSTM1 and UB, this undoubtedly confirms there happened autophagic hyperactivity. Specially, the chemical inhibition of autophagy could clearly salvage the levels of PtdIns(4,5)P$_2$, p-CFL1 (Ser3) and ACTR2, as well as the morphology of MTOC and spindle. Therefrom we assume that the autophagic activity is grossly enhanced in response to the loss of PLD1 function, thus definitely speeds up the degradation of PtdIns(4,5)P$_2$, p-CFL1 (Ser3) and ACTR2. Previous studies show that dysregulational autophagy impacts spindle migration in mouse oocytes [16], and centrosome composition in U2OS cells [17], however the molecular mechanism underlying these morphological changes is not explored. We believe this is largely concerned with damaged stability of PtdIns(4,5)P$_2$, p-CFL1 (Ser3) and ACTR2 under the condition of hyperfunctional autophagy.

It has been demonstrated that MTOR signal pathway is negatively associated with autophagy activation, and MTOR inhibitors can stimulate antophagic flux [14–17]. We found the blocking of PLD1 could inactivate MTOR signaling, through inhibiting MTOR phosphorylation and its downstream target RPS6KB. This is in line with previous assumption that PLD1 is a critical regulator of MTOR activation by a variety of stimuli [29,32]. PLD1 product phosphatidic acid physically associates with the FKBP12-rapamycin-binding (FRB) domain of MTOR encompassing amino acids 2015–2114, located N-terminal to the kinase domain [32]. Roughly speaking, PLD1 activity is consistent with MTOR pathway in suppressing autophagy. In addition, we notice the autophagic signal is specially absent in the cytoplasmic area of spindle structure, this pattern was broken upon PLD1 inhibition. The distributional asymmetry indicates that PLD1 may work to maintain the regional specificity of autophagic activity, thus promote enough stability of some elements, such as PtdIns(4,5)P$_2$, p-CFL1 (Ser3) and ACTR2, around spindle apparatus.

In summary, data presented here suggest that PLD1 facilitates the spindle assembly and cortical migration through maintaining reasonable levels of PtdIns(4,5)P$_2$, p-CFL1 (Ser3) and ACTR2 in a manner of regulating autophagy flux in mouse oocyte meiosis. These findings have important implications for the unique activity status and function of autophagic flux during oocyte meiotic division, and provide a valuable insight into the molecular mechanisms of spindle assembly and migration in mammalian oocyte meiosis.

Materials and methods

Oocyte collection and in vitro culture

All the animal experiments were strictly conducted following the policies and instructions of the Care and Use of Animals in Research and Teaching and approved by the Animal Care and Use Committee of Capital Medical University with the approval No. AEEI-2020-151. To collect fully-grown GV oocytes, 21–23 days old CB6F1 (C57BL/6 BALB/C F1) female mice were injected with 10 IU pregnant mare serum gonadotropin (PMSG; Ningbo Second Hormone Factory 110,254,564) to stimulate preovulatory follicle development. After 44–48 h, the mice were euthanatized with CO$_2$ and the cumulus oocyte complexes (COCs) were isolated and incubated in minimum essential medium alpha (MEM α; Gibco 12,571–063) containing 3 mg/ml bovine serum albumin (BSA; Sigma-Aldrich, A1933) and 10% fetal bovine serum (FBS; Gibco 10,099) at 37°C in a humid atmosphere with 5% CO$_2$. At different time points during culture, oocytes were denuded by gentle mechanical pipetting and collected for subsequent analysis.

Microinjection and morpholino oligo interference

Fully-grown GV oocytes were microinjected with 10–15 pl of 1 mM *Ctrl* (5'-CCTCTTACCTCAGTTACAATTTATA-3', Gene Tools) or *Pld1* morpholino oligo (5'-GTCTCGCTTTTCAGTGACATGCTAG-3', Gene Tools) in MEM-HEPES medium (Gibco 42,360–032) containing 2.5 μM milrinone (Selleck, S2484). To facilitate the degradation of protein, microinjected oocytes were maintained at GV arrest in MEM α medium for 28 h, and then transferred to milrinone-free M16 medium (Sigma-Aldrich, M7292) to resume the meiosis for further experiments.

cRNA construction and in vitro transcription

Wild-type full-length *Pld1*, *Pld1^{F120A,R179Q}*, *Pld1^{K898R}*, *Cfl1^{S3A}*, *Cfl1^{S3E}* and wild-type full-length *Actr2* cDNA were subcloned into pCS2+/myc vectors (gifts from Prof. Zhenbo Wang, Institute of Zoology, Chinese Academy of Sciences) by Beijing Likeli Biotechnology Company. Plasmids were extracted using EndoFree Plasmid Midi Kit (CWBIO, CW2105S) and linearized by AscI (NEB, R0558L). cRNA was synthesized from linearized plasmid using SP6 mMessage mMachine kit (Thermo Fisher Scientific, AM1340), and purified with Monarch® RNA cleanup kit (NEB, T2040L). After microinjected with 10–15 pl of 1000–1500 ng/μl cRNA, oocytes were arrested at the GV stage for 8–12 h for effective peptide synthesis, and then cultured in milrinone-free M16 medium for further analysis.

Drug treatment

VU 0155069 (Santa Cruz Biotechnology, sc -224,371) and Baf-A1 (MCE, HY-100558) were dissolved in dimethylsulfoxide

MO and *Pld1* MO + *myc-Actr2*, respectively. Arrowheads indicated concentration of TUBG on spindle poles. Red, TUBG; green, acetylated-TUBA; blue, DNA. Scale bar: 20 μm. (C-I) statistical analysis of spindle migration (d1/R), relative area of spindle (%), spindle length (l/R), width of chromosome region (d2/R), oocytes with asymmetrical spindle (%), oocytes with defocused polar MTOC (%) and numbers of MTOC dots in poles in different groups. *ctrl* MO group: n = 113, *Pld1* MO group: n = 115, *Pld1* MO + *myc-Actr2* group: n = 116. (J) statistical analysis of relative size of PB1(%) in *ctrl* MO (n = 103), *Pld1* MO (n = 100) and *Pld1* MO + *myc-Actr2* (n = 100) groups. (K) Representative images of MI oocytes in groups of *ctrl* MO, *Pld1* MO and *Pld1* MO + *myc-Actr2*. Arrowheads indicated aggregations of GOLGA2 and RAB11A in cytoplasm. Red, RAB11A; green, GOLGA2; blue, DNA. Scale bar: 20 μm. (L, M) statistical analysis of numbers of large RAB11A-positive vesicles (>1000 pixels) and small RAB11A-positive vesicles (<1000 pixels) in different groups. *ctrl* MO group: n = 114, *Pld1* MO group: n = 116, *Pld1* MO+ *myc-Actr2* group: n = 118. All data were presented as the mean percentage (mean ± SEM) of at least three independent experiments. ***p < 0.01, ****p < 0.001, ****p < 0.0001 by ordinary one-way ANOVA analysis.
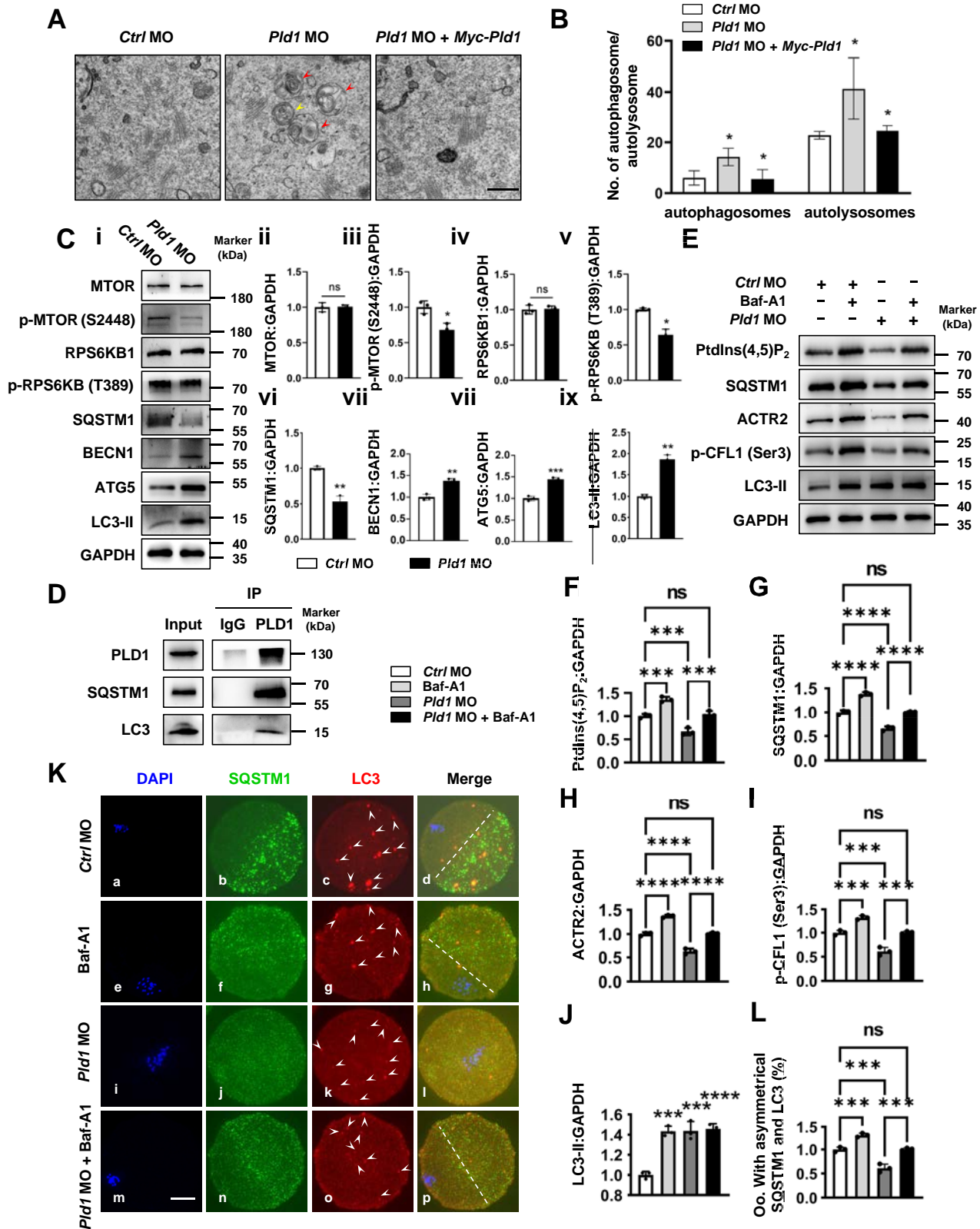
Figure 10. PLD1 depletion enhanced autophagy. (A) Representative transmission electron microscopy (TEM) images of MI oocytes in groups of *ctrl* MO, *Pld1* MO and *Pld1* MO + *myc-Pld1*, respectively.Yellow arrowheads showed autophagosomes, red arrowheads showed autolysosomes. Scale bar: 500 nm. (B) statistical analysis of numbers of autolysosomes in *ctrl* MO (n = 4), *Pld1* MO (n = 4) and *Pld1* MO + *myc-Pld1* (n = 4) groups. (C-i) expression of MTOR, p-MTOR (S2448) , RPS6KB1, p-RPS6KB (T389), SQSTM1, LC3-II, ATG5 and BECN1 in oocytes in *ctrl* MO and *Pld1* MO group by western blot. Each sample had 80 oocytes. (C-ii-vii) quantitative analysis of protein level changes in oocytes. (D) Co-IP was performed to determine the interaction between PLD1 and SQSTM1, LC3. Oocytes lysates were incubated with IgG or anti-PLD1 antibody. The blots of IP eluates were probed with anti-PLD1, anti-SQSTM1 and anti-LC3 antibodies, respectively. (E) expression of PtdIns(4,5)P$_2$, SQSTM1, ACTR2, p-CFL1 (Ser3) and LC3 in oocytes in groups of *ctrl* MO, baf-A1, *Pld1* MO and *Pld1* MO + baf-A1 by western blot. Each sample had 80 oocytes. (F-J) quantitative analysis of protein level changes in oocytes. (K) Representative images of MI oocytes in groups of *ctrl* MO, baf-A1, *Pld1* MO and *Pld1* MO + baf-A1, respectively. Arrowheads indicated patch-like aggregations of LC3 in cytoplasm; the dashed line displayed the regional specificity of autophagy signal distribution. Red, LC3; green, SQSTM1; blue, DNA. Scale bar: 20 μm. (L) quantitative analysis of oocytes with asymmetrical distribution of SQSTM1 and LC3(%). *ctrl* MO group: n = 101, baf-A1 group: n = 111, *Pld1* MO group: n = 121, *Pld1* MO + baf-A1 group: n = 116. All data were presented as the mean percentage (mean ± SEM) of at least three independent experiments. ***p < 0.05, ****p < 0.01, ****p < 0.001, ***p < 0.0001, by unpaired t test or ordinary one-way ANOVA analysis.
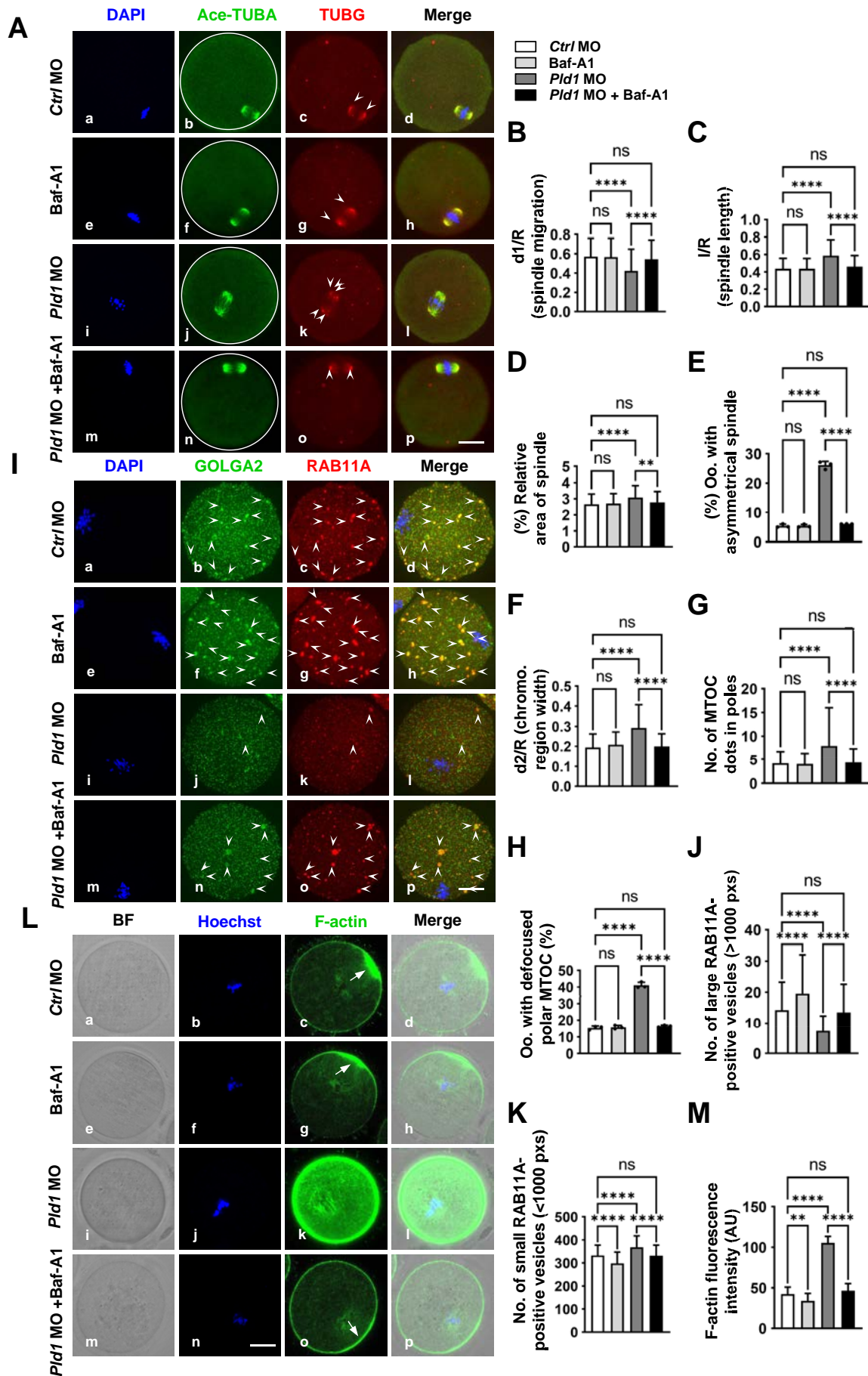
Figure 11. Autophagy inhibition could rescue spindle assembly and migration failure caused by PLD1 depletion. (A) Representative images of MTOC (red), spindle (green) and chromosomes (blue) in MI oocytes from groups of *ctrl* MO, baf-A1, *Pld1* MO and *Pld1* MO + baf-A1 groups, respectively. Arrowheads indicated signal of
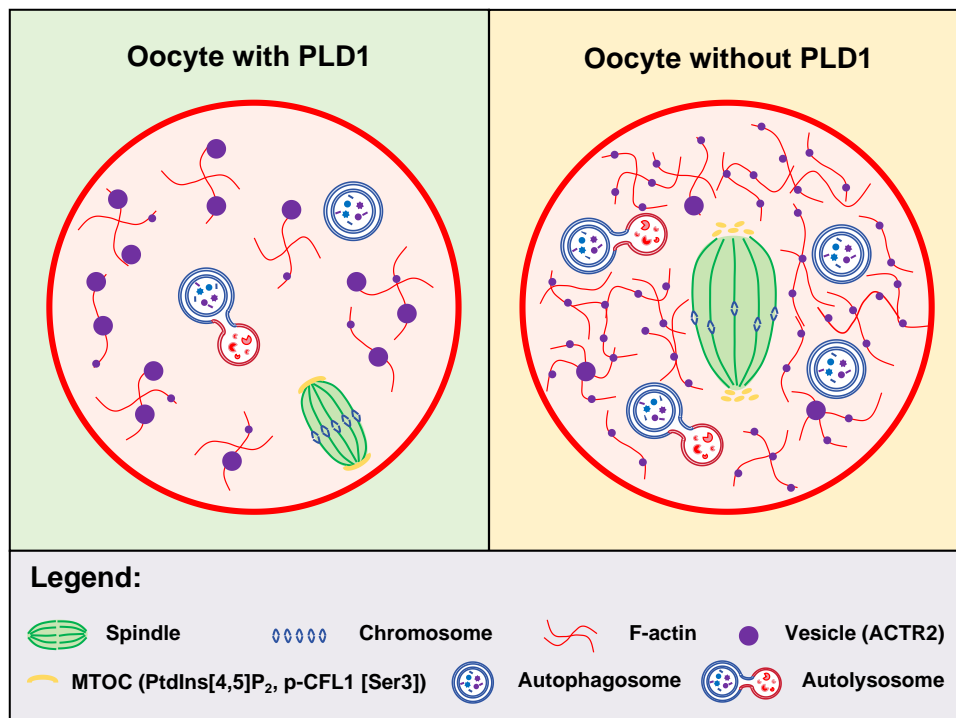
Figure 12. A schematic diagram depicting roles of PLD1 in mouse oocyte meiosis. Left panel, in the presence of PLD1, autophagy is maintained at rational level, spindle assembly and cortical migration orderly occur in oocyte meiosis. Right panel, in the absence of PLD1, autophagy is hyperfunctional, spindle assembly and migration are destroyed by defective changes in MTOC clustering, vesicle fusion and F-actin assembly, due to reduction in ACTR2, PtdIns(4,5)P$_2$ and p-CFL1 (Ser3).

(DMSO; Sigma-Aldrich 276,855) to 10 mM or 200 μM for stock solutions, which were further diluted in culture medium to the working concentration, respectively. PtdIns(4,5)P$_2$ (Echelon Biosciences, p-4508) were dissolved in ddH$_2$O to 25 mM for stock solutions which was further diluted in culture medium to the working concentration. GV oocytes were treated with these inhibitors in MEM α at 37°C. Oocytes in control group were treated with the same concentration of DMSO or ddH$_2$O.

Antibodies

Rabbit anti-PLD1 antibody, rabbit anti-CFL1 antibody, rabbit anti-phospho-CFL1 (Ser3) antibody, rabbit anti-LC3A/B antibody, rabbit anti-phospho-RPS6KB (T389) and rabbit anti-BECN1 antibody were purchased from Cell Signaling Technology (3832, 5175, 3313, 4108, 9234 and 3495), rabbit polyclonal anti-phospho-CFL1 (Ser3) antibody was from GeneTex (GTX50199), mouse monoclonal anti-PtdIns(4,5)P$_2$ antibody was from Echelon Biosciences (Z-P045), mouse monoclonal anti-ACTR2 antibody and mouse anti-ATG5 antibody were purchased from Santa Cruz Biotechnology (sc -166,103 and sc -133,158),

rabbit monoclonal anti-ACTR3 antibody, rabbit polyclonal anti-TUBG antibody, mouse polyclonal anti-SQSTM1 antibody and rabbit polyclonal anti-RPS6KB1 antibody were purchased from Abcam (ab181164, ab179503, ab56416 and ab32529), rabbit polyclonal anti-FMN2 antibody, rabbit polyclonal anti-RAB11A antibody, rabbit polyclonal anti-MTOR antibody and rabbit polyclonal anti-MTOR (S2448) antibody were purchased from Proteintech (11259–1-AP 20,229–1-AP 66,888–1-AP and 67,778–1-AP), mouse monoclonal anti-acetylated TUBA (lysine-40) antibody and rabbit polyclonal anti-GAPDH (glyceraldehyde-3-phosphate dehydrogenase) antibody were from Sigma-Aldrich (T7451 and SAB4300645), mouse monoclonal anti-GOLGA2 was from BD Biosciences (610823), mouse monoclonal anti-TUBA antibody was from ABclonal (AC012), mouse monoclonal anti-MYC antibody was from TransGen Biotechnology (HT101–01), Alexa Fluor 488-conjugated goat anti-mouse IgG (H + L), Alexa Fluor 594-conjugated goat anti-rabbit IgG (H + L), HRP-conjugated goat anti-rabbit IgG (H + L) and HRP-conjugated goat anti-mouse IgG (H + L) were purchased from Zhongshan Golden Bridge Biotechnology (ZF-0512, ZF-0516, ZB-2301 and ZB-2305).

TUBG on spindle poles. Scale bar: 20 μm. (B-H) statistical analysis indicates difference in spindle migration (d1/R), relative area of spindle (%), spindle length (l/R), oocytes with asymmetrical spindle (%), width of chromosome region (d2/R), oocytes with defocused polar MTOC (%), numbers of MTOC dots in poles and asymmetrical spindle among different groups. *ctrl* MO group: $n = 120$, baf-A1 group: $n = 115$, *Pld1* MO group: $n = 113$, *Pld1* MO + baf-A1 group: $n = 120$. (I) Representative images of vesicles in MI oocytes from groups of *ctrl* MO, baf-A1, *Pld1* MO and *Pld1* MO + baf-A1, respectively. Arrowheads displayed the aggregations of GOLGA2 and RAB11A. Red, RAB11A; green, GOLGA2; blue, DNA. Scale bar: 20 μm. (J, K) statistical analysis of numbers of large RAB11A-positive vesicles (>1000 pixels) and small RAB11A-positive vesicles (<1000 pixels) in different groups. *ctrl* MO group: $n = 120$, baf-A1 group:$n = 120$, *Pld1* MO group: $n = 114$, *Pld1* MO + baf-A1 group: $n = 120$. (L) Representative images of F-actin in MI oocytes from different groups. Arrow indicated actin cap on cytoplasmic membrane. Green, F-actin; blue, DNA. Scale bar: 20 μm. (M) statistical analysis of F-actin fluorescence intensity (AU) in different groups. *ctrl* MO group: $n = 32$, baf-A1 group: $n = 31$, *Pld1* MO group: $n = 33$, *Pld1* MO + baf-A1 group: $n = 32$. All data were presented as the mean percentage (mean ± SEM) of at least three independent experiments. ***$p < 0.01$, ****$p < 0.0001$ by ordinary one-way ANOVA analysis.

Immunofluorescence and microscopy

Oocytes were fixed in 1% paraformaldehyde (Sigma-Aldrich 158,127) in PEM buffer (100 mM PIPES, pH 6.9, 1 mM MgCl$_2$, 1 mM EGTA) with 0.5% Triton X-100 (Sigma-Aldrich, T8787) for 45 min at room temperature, then washed in phosphate-buffered saline (PBS; Sigma-Aldrich, P5493) with 0.02% Triton X-100 (PBST), 5 min each. Alternatively, oocytes were fixed in 1% paraformaldehyde in PEM buffer for 30 min, and then permeated in 0.5% Triton X-100 for 5 min at room temperature. The fixed oocytes were blocked for 1 h in PBS supplemented with 1% BSA, 2.28% glycine, 0.02% Triton X-100, and 10% normal goat serum (NGS; Zhongshan Golden Bridge Biotechnology, ZLI-9021), and incubated in blocking buffer with primary antibodies at 4°C overnight. Oocytes were then washed three times, each for 15 min, in PBST, and labeled with appropriate secondary antibodies for 1 h at room temperature. After being washed thoroughly, the oocytes were mounted on glass slides in mountain medium with 6-diamidino-2-phenylindole (DAPI; Vector laboratories, H-1200). The fluorescent signals from both control and experimental oocytes were acquired by setting up the same parameters of the upright fluorescent microscope (ZEISS Axio Imager A2) and semi-quantitatively analyzed by Image-Pro Plus software.

F-actin staining and live cell imaging

MI stage oocytes were incubated with MEM medium containing Hoechst 33,342 (1 μg/ml, Cell Signaling Technology, 4082) and Cell mask green actin tracking stain (200 nM, Invitrogen, A57243) for 30 min. After washed six times by HEPES-MEM medium, pre-labeled oocytes were transfered into 10 μl MEM medium drop covered under mineral oil in a 20-mm glass bottom culture dish. Images were acquired with LSM 880 with Airyscan confocal laser scanning microscopes (Zeiss) equipped with 63×C-Apochromat, 1.4 NA oil immersion objective. Hoechst was excited with a 405-nm laser line and detected at 355 to 465 nm, F-actin was excited with a 488-nm laser line and detected at 503 to 512 nm. Images of the control and experimental groups were acquired under identical imaging conditions on the same microscope.

Western blot

A total of 50–200 oocytes were lysed directly in Laemmli sample buffer (BIO-RAD 1,610,737) with β-mercaptoethanol (Sigma-Aldrich, M6250) and protease inhibitor cocktail (MCE, HY-K0016), and heated at 100°C for 10 min. The protein samples were separated on 10% SDS-PAGE gel at 110 V for 1.5 h, transferred to the polyvinylidene fluoride (PVDF) membrane (Millipore 03,010,040,001) at 250 mA for 2 h. Non-specific blots were blocked in Tris-buffered saline (0.05% MgCl$_2$, 150 mM NaCl, 10 mM Tris base, pH 7.4) with 0.1% Tween 20 (Applygen, A1007; TBST) containing 5% skimmed milk (Applygen, P1622) or 5% BSA for 1 h at room temperature. The membrane was incubated in primary antibody at 4°C overnight and then washed three times in TBST, 15 min each, followed by incubation with secondary antibody for 1 h at room temperature. The blots were detected with appropriate amount of ECL Plus Substrate (Vazyme, E423–01/02). The relative signal intensities of immunoreactive bands were analyzed using gel software Image Lab 3.0.

Immunoprecipitation

Immunoprecipitation (IP) was performed using the Pierce Crosslink Magnetic IP/Co-IP Kit (Thermo Fisher Scientific 88,805). According to the manufacturer's protocol, beads were pre-washed two times with Modified Coupling Buffer, then incubated with antibody for 15 min, followed by three washes with Modified Coupling Buffer. After the antibody to beads was crosslinked with DSS for 30 min, the beads were washed three times with Elution Buffer and subsequent two washes with IP Lysis/Wash Buffer. Cellular lysates were prepared by incubating the cells in IP Lysis/Wash Buffer containing protease inhibitor cocktail (MCE, HY-K0010), and then incubated with antibody-crosslinked beads for 2 h at room temperature. After that, the beads were washed two times with IP Lysis/Wash Buffer and one time with ultrapure water. The precipitated antigens were eluted from the beads by resuspending the beads in Elution Buffer and boiling for 10 min, then detected by western blot procedure.

Proximity ligation assay

Proximity ligation assay (PLA) was performed using the Duolink® In situ Red Starter Kit Mouse/Rabbit (Sigma-Aldrich, DUO92105). According to the manufacturer's instructions, oocytes were pre-processed with a sequence of fixation, recovery and permeabilization, similar with the immunofluorescence staining introduced above. The oocytes were blocked with Duolink® block buffer at 37°C for 1 h, and incubated with rabbit anti-PLD1 antibody, mouse anti-GOLGA2 antibody, rabbit anti-RAB11A antibody + mouse anti-GOLGA2 antibody, rabbit anti-PLD1 antibody + mouse anti-GOLGA2 antibody, overnight at 4°C, then followed by 1 h treatment in prediluted anti-rabbit plus and anti-mouse minus probes at 37°C. Thereafter, the oocytes were consecutively incubated in 1×ligase and 1×polymerase, for 30 and 100 min, respectively, at 37°C, and then mounted on the slides with Duolink® In situ Mounting Medium with DAPI.

Transmission electron microscopy (TEM)

Oocytes were fixed in 2.5% glutaraldehyde (Sigma-Aldrich, G5882) for at least 2 days at 4°C, and then treated with 1% agar (Sigma-Aldrich, A1296) for 40 min and dehydrated in ascending series of ethanol. After that, oocytes were immersed in propylene oxide for solvent substitution, embedded in Epon 812 (Agar Scientific, R1045) and sectioned. Ultrathin sections (60–80 nm) were cut with a diamond knife, mounted on copper grids and contrasted with saturated uranyl acetate followed by lead citrate. Grids were examined and photographed using a FEI Tecnai 8482 Electron Microscope operating at 120 kV.

Statistical analysis

The data were expressed as the mean ± SEM of a minimum of three independent experimental replicates. Differences between treated groups were analyzed by t-test or one-way ANOVA using GraphPad Prism 9.3.1 software (Hallogram Publishing, USA), and the level of significance was accepted as $p < 0.05$.

Acknowledgements

Disclosure statement

Funding

References

[1] Coticchio G, Dal Canto M, Mignini Renzini M, et al. Oocyte maturation: gamete-somatic cells interactions, meiotic resumption, cytoskeletal dynamics and cytoplasmic reorganization. Hum Reprod Update. 2015 Jul-Aug;21(4):427–454.

[2] Duan X, Li Y, Yi K, et al. Dynamic organelle distribution initiates actin-based spindle migration in mouse oocytes. Nat Commun. 2020 Jan 14;11(1):277. doi: 10.1038/s41467-019-14068-3

[3] Uraji J, Scheffler K, Schuh M. Functions of actin in mouse oocytes at a glance. J Cell Sci. 2018 Nov 22;131(22). doi: 10.1242/jcs.218099

[4] Azoury J, Lee KW, Georget V, et al. Spindle positioning in mouse oocytes relies on a dynamic meshwork of actin filaments. Curr Biol. 2008 Oct 14;18(19):1514–1519. doi: 10.1016/j.cub.2008.08.044

[5] Li H, Guo F, Rubinstein B, et al. Actin-driven chromosomal motility leads to symmetry breaking in mammalian meiotic oocytes. Nat Cell Biol. 2008 Nov;10(11):1301–8. doi: 10.1038/ncb1788

[6] Schuh M, Ellenberg J. A new model for asymmetric spindle positioning in mouse oocytes. Curr Biol. 2008 Dec 23;18(24):1986–1992. doi: 10.1016/j.cub.2008.11.022

[7] Sun SC, Wang ZB, Xu YN, et al. Arp2/3 complex regulates asymmetric division and cytokinesis in mouse oocytes. PloS One. 2011 Apr 8;6(4):e18392. doi: 10.1371/journal.pone.0018392

[8] Holubcova Z, Howard G, Schuh M Vesicles modulate an actin network for asymmetric spindle positioning. Nat Cell Biol. 2013 Aug;15(8):937–47. doi: 10.1038/ncb2802

[9] Schuh M. An actin-dependent mechanism for long-range vesicle transport. Nat Cell Biol. 2011 Oct 9;13(12):1431–6. doi: 10.1038/ncb2353

[10] Schuh M, Ellenberg J. Self-organization of MTOCs replaces centrosome function during acentrosomal spindle assembly in live mouse oocytes. Cell. 2007 Aug 10;130(3):484–98. doi: 10.1016/j.cell.2007.06.025

[11] Terry Hassold PH, Hunt P To err (meiotically) is human: the genesis of human aneuploidy. Nat Rev Genet. 2001 April;2(4):280–291. doi: 10.1038/35066065

[12] Konotop G, Bausch E, Nagai T, et al. Pharmacological inhibition of centrosome clustering by slingshot-mediated cofilin activation and actin cortex destabilization. Cancer Res. 2016 Nov 15;76(22):6690–6700. doi: 10.1158/0008-5472.CAN-16-1144

[13] Gorbatyuk VY, Nosworthy NJ, Robson SA, et al. Mapping the phosphoinositide-binding site on chick cofilin explains how PIP2 regulates the cofilin-actin interaction. Mol Cell. 2006 Nov 17;24(4):511–522. doi: 10.1016/j.molcel.2006.10.007

[14] Boya FraPC P, Reggiori F, Codogno P Emerging regulation and functions of autophagy. Nat Cell Biol. 2013 July;15(7):713–721. doi: 10.1038/ncb2788

[15] HM VJ, Kawabata T, Youle RJ, et al. The mechanisms and roles of selective autophagy in mammals. Nat Rev Mol Cell Biol. 2023 Mar; 24;24(3):167–185. doi: 10.1038/s41580-022-00542-2

[16] Lee SE, Sun SC, Choi HY, et al. mTOR is required for asymmetric division through small GTPases in mouse oocytes. Mol Reprod Dev. 2012 May;79(5):356–366.

[17] Holdgaard SG, Cianfanelli V, Pupo E, et al. Selective autophagy maintains centrosome integrity and accurate mitosis by turnover of centriolar satellites. Nat Commun. 2019 Sep 13;10(1):4176. doi: 10.1038/s41467-019-12094-9

[18] Bowling FZ, Frohman MA, Airola MV Structure and regulation of human phospholipase D. Adv Biol Regul. 2021 Jan;79:100783. doi: 10.1016/j.jbior.2020.100783

[19] Exton JH. Phospholipase D: enzymology, mechanisms of regulation, and func tion. Physiol Rev. 1997;77:303–320. doi: 10.1152/physrev.1997.77.2.303

[20] Park SY, Han JS Phospholipase D1 signaling: essential roles in neural stem cell differentiation. J Mol Neurosci. 2018 Mar;64(3):333–340. doi: 10.1007/s12031-018-1042-1

[21] Barber CN, Huganir RL, Raben DM Phosphatidic acid-producing enzymes regulating the synaptic vesicle cycle: role for PLD? Adv Biol Regul. 2018 Jan;67:141–147. doi: 10.1016/j.jbior.2017.09.009

[22] Rudge SA, Wakelam MJ Inter-regulatory dynamics of phospholipase D and the actin cytoskeleton. Biochim Biophys Acta. 2009 Sep;1791(9):856–861. doi: 10.1016/j.bbalip.2009.04.008

[23] Tu-Sekine B, Goldschmidt H, Raben DM Diacylglycerol, phosphatidic acid, and their metabolic enzymes in synaptic vesicle recycling. Adv Biol Regul. 2015 Jan;57:147–152. doi: 10.1016/j.jbior.2014.09.010

[24] Roth KB MG, Ktistakis NT, Yu S. Phospholipase D as an effector for ADP-ribosylation factor in the regulation of vesicular traffic. Chem Phys Lipids. 1999;98(1–2):141–152. doi: 10.1016/S0009-3084(99)00026-2

[25] Field SJ, Madson N, Kerr ML, et al. PtdIns(4,5)P2 functions at the cleavage furrow during cytokinesis. Curr Biol. 2005 Aug 9;15(15):1407–1412. doi: 10.1016/j.cub.2005.06.059

[26] Senju Y, Lappalainen P Regulation of actin dynamics by PI(4,5)P2 in cell migration and endocytosis. Curr Opin Cell Biol. 2019 Feb;56:7–13. doi: 10.1016/j.ceb.2018.08.003

[27] Oude Weernink PA, Lopez de Jesus M, Schmidt M. Phospholipase D signaling: orchestration by PIP2 and small GTPases. Naunyn Schmiedebergs Arch Pharmacol. 2007 Feb;374(5–6):399–411. doi: 10.1007/s00210-007-0131-4

[28] Ali WH, Chen Q, Delgiorno KE, et al. Deficiencies of the lipid-signaling enzymes phospholipase D1 and D2 alter cytoskeletal organization, macrophage phagocytosis, and cytokine-stimulated neutrophil recruitment. PLoS One. 2013;8(1):e55325. doi: 10.1371/journal.pone.0055325

[29] Fang Y, Park IH, Wu AL, et al. PLD1 regulates mTOR signaling and mediates Cdc42 activation of S6K1. Curr Biol. 2003 Dec 2;13(23):2037–2044. doi: 10.1016/j.cub.2003.11.021

[30] Cai M, He J, Xiong J, et al. Phospholipase D1-regulated autophagy supplies free fatty acids to counter nutrient stress in cancer cells. Cell Death Dis. 2016 Nov 3;7(11):e2448. doi: 10.1038/cddis.2016.355

[31] Dall'armi C, Hurtado-Lorenzo A, Tian H, et al. The phospholipase D1 pathway modulates macroautophagy. Nat Commun. 2010;1(1):142. doi: 10.1038/ncomms1144

[32] Sun Y, Chen J mTOR signaling: PLD takes center stage. Cell Cycle. 2008 Oct;7(20):3118–23. doi: 10.4161/cc.7.20.6881

[33] Guizzunti G, Seemann J. Mitotic golgi disassembly is required for bipolar spindle formation and mitotic progression. Proc Natl Acad Sci U S A. 2016 Oct 25;113(43):E6590–E6599. doi: 10.1073/pnas.1610844113

[34] Misteli T. Molecular mechanisms in the disassembly and reassembly of the mammalian golgi apparatus during M-phase. FEBS Lett. 1996 Jun 24;389(1):66–69. doi: 10.1016/0014-5793(96)00518-2

[35] Wang E, Pennington JG, Goldenring JR, et al. Brefeldin a rapidly disrupts plasma membrane polarity by blocking polar sorting in common endosomes of MDCK cells. J Cell Sci. 2001;114:3309–3321. doi: 10.1242/jcs.114.18.3309

[36] Zhou K, Sumigray KD, Lechler T, et al. The Arp2/3 complex has essential roles in vesicle trafficking and transcytosis in the mammalian small intestine. Mol Biol Cell. 2015 Jun 1;26 (11):1995–2004. doi: 10.1091/mbc.E14-10-1481

[37] Rajat Rohatgi LM, Miki H, Lopez M, et al. The interaction between N-WASP and the Arp2,3 complex links CDC42-dependent signals to actin assembly. Cell. 1999 April 16;97:221–231. doi: 10.1016/S0092-8674(00)80732-1

[38] Namgoong S, Kim NH. Roles of actin binding proteins in mammalian oocyte maturation and beyond. Cell Cycle. 2016 Jul 17;15 (14):1830–43. doi: 10.1080/15384101.2016.1181239

[39] Kang DE, Woo JA, Reddy PH. Cofilin, a Master node regulating cytoskeletal pathogenesis in Alzheimer's Disease. J Alzheimers Dis. 2019;72(s1):S131–S144. doi: 10.3233/JAD-190585

[40] Molli PR, Li DQ, Bagheri-Yarmand R, et al. Arpc1b, a centrosomal protein, is both an activator and substrate of Aurora A. J Cell Bio. 2010 Jul 12;190(1):101–114. doi: 10.1083/jcb.200908050

[41] Plessner M, Knerr J, Grosse R. Centrosomal actin assembly is required for proper mitotic spindle formation and chromosome congression. iScience. 2019 May 31;15:274–281. doi: 10.1016/j.isci.2019.04.022

[42] Farina F, Gaillard J, Guerin C, et al. The centrosome is an actin-organizing centre. Nat Cell Biol. 2016 Jan;18(1):65–75.